



ELSEVIER

Contents lists available at ScienceDirect

Engineering Failure Analysis

journal homepage: www.elsevier.com/locate/engfailanal

Analysis of failure modes in pipe-in-pipe repair systems for water and gas pipelines

T. Tafsirojjaman^{a,*}, Allan Manalo^a, Cam Minh Tri Tien^a, Brad P. Wham^b,
Ahmad Salah^a, Shanika Kiriella^a, Warna Karunasena^a, Patrick Dixon^b

^a Centre for Future Materials (CFM), School of Engineering, University of Southern Queensland (USQ), Toowoomba QLD-4350, Australia

^b Center for Infrastructure, Energy, and Space Testing, University of Colorado Boulder, 1111 Engineering Drive, UCB 428 ECOT 428, Boulder, CO 80309, USA

ARTICLE INFO

Keywords:

Pipe-in-pipe systems
Performance objectives
Failure modes
Analytical Hierarchy Process

ABSTRACT

Different failure modes should be carefully analyzed to effectively design the pipe-in-pipe (PIP) repair systems to rehabilitate natural gas and water pipelines in place and in service. This study characterizes the failure modes through analytical and numerical modelling of the different performance objectives to have a comprehensive understanding of the overall behavior of PIP systems with a range of thicknesses and elastic moduli. It focused on assessing the structural performance of PIP systems under different load actions including vibration/fatigue due to traffic loads, lateral deformation, cross-section ovalization, axial stresses and thermal deformation, internal pressure, and impact. The results of the analyses showed that the thickness and elastic modulus significantly affect the failure modes of PIP systems. The implemented Analytical Hierarchy Process (AHP) suggested that lateral deformation is the most critical failure mode followed by internal pressure based on global priority as well as both criteria (thickness and elastic modulus) when the design pressure is 200 psi with the cross-section ovalization the least critical failure mode of the PIP systems. The results of this study provide useful predictive modelling techniques and preliminary design tools for PIP systems for new material systems development and/or evaluation of the suitability of the available PIP systems for pipeline repair.

1. Introduction

Critical natural gas service is supplied to nearly 80 million customers in the U.S. [1] through a network of 2 million miles (3.2 million kms) of utility pipes [2]. This essential distribution system, much of which is composed of legacy cast iron and bare steel pipelines at or beyond their intended design life, needs cost-effective repair techniques to extend its safe operating life. The rehabilitation of underground pipes is currently implemented either through open trench methods or trenchless methods. The trenchless method has become the most popular pipe repair technology in many countries such as the USA and Canada as they reduce environmental damages and minimize excavation activities which make them more reliable and cost-effective [3]. This repair method has developed rapidly in recent years using different techniques (such as Pipe-in-Pipe System or PIPs) and different material systems (such

* Corresponding author.

E-mail addresses: tafsirojjaman@usq.edu.au (T. Tafsirojjaman), allan.manalo@usq.edu.au (A. Manalo), camminhtri.tien@usq.edu.au (C.M.T. Tien), brad.wham@colorado.edu (B.P. Wham), ahmad.salah@usq.edu.au (A. Salah), shanika.kiriella@usq.edu.au (S. Kiriella), karu.karunasena@usq.edu.au (W. Karunasena), padi9036@colorado.edu (P. Dixon).

<https://doi.org/10.1016/j.engfailanal.2022.106510>

Received 28 February 2022; Received in revised form 7 May 2022; Accepted 31 May 2022

Available online 4 June 2022

1350-6307/© 2022 The Authors. Published by Elsevier Ltd. This is an open access article under the CC BY license (<http://creativecommons.org/licenses/by/4.0/>).

as fiber reinforced polymer composites and polymeric coatings). New technologies required to rehabilitate cast iron, wrought iron, and bare steel natural gas distribution pipes require a detailed understanding of their failure mechanisms to be designed appropriately and to operate throughout their service life without reliance on the exterior host pipe.

Failures in gas and oil pipelines can cause catastrophic damage to properties, lives, and infrastructure due to their combustibility of the contained material [4]. On the 9th of September 2010, a rupture, which occurred in the gas pipe in San Bruno, California, resulted in eight dead and significant loss of property [5]. In addition, Lu et al. [6] listed more than 200 people killed and 500 significantly injured between 2011 and 2017 in major oil and gas pipeline accidents in the world. Further investigations by The National Transportation Safety Board showed brittle pipe, old welds, corrosion or cracks caused the pipe failure [7]. \$11 billion dollars was estimated as the cost of an upgraded safety program of California pipeline owned by Pacific Gas and Electric Company [5]. Failure modes occur with the deterioration of existing systems and aging civil infrastructure, which have been subjected to material degradation, corrosion, environmental attack, impact damage and increases in internal pressure and surface traffic [8–12]. Due to limited financial resources, rehabilitation of existing pipe networks and infrastructure systems is a preferred solution to replacement [13]. This has led to research and development of different repair technologies. Sirimanna et al. [14] provided an extensive overview of internal composite repair technologies for corroded pipelines and evaluated their suitability in terms of their maximum allowable working pressure, pipe diameter and service temperature. The impact resistance of PIP is reduced due to corrosion defects under transverse impact load and aggravated the damage of inner pipe [15]. The structural performance of the PIP system can be also affected by the presence of residual stress in the carrier and inner pipes, induced during the assembly procedure [16]. Moreover, the different service pipes are subjected to vibrational load during the operation due to the turbulence in the flow which may easily result the failures [17]. Li et al. [18] found substantial reductions in critical pressure with pipes of variable wall thickness. Similarly, Lu et al. [6] summarizes the characteristics and applications of mature trenchless technologies for oil and gas pipes. Based on these state-of-the-art reviews, various trenchless methods have become relatively mature, but there remain certain limitations in their application to oil and gas pipelines due to their limited technical adaptability and high cost of installation.

In the internal repair systems to rehabilitate pipelines in place and in service, different Performance Objectives (POs), and associated Failure Mechanisms (FMs), should be considered to effectively design PIP systems. Unfortunately, there are currently no comparable regulations nor standards for pipe-in-pipe repair systems. POs for PIPs are not fully understood as many long-term influential factors are difficult to study experimentally. For example, structural PIP systems should have sufficient modulus of elasticity in the longitudinal direction to accommodate bending deflection and in the radial direction to overcome ovalization/buckling. Lu et al. [6] highlighted that repair materials are important consideration when selecting a specific trenchless method. This ensures the suggested PIP systems have sufficient material properties to operate throughout their service life without reliance on the exterior pipe. Related literature shows that the loading conditions have significant effects on the failure mechanism of the host pipes and PIP system. Fatigue failure [19,20], crack propagation [21–23] and buckling due to lateral deformation [24–27], localized failures and leakage due to internal pressure [28–30] and axial deformation due to thermal stresses [19,31] are found as the common failure modes for the host pipes and PIP system. Many experimental studies and finite element (FE) analyses have been conducted to select the appropriate parameters design (i.e. repair thickness and composite material structure), the behaviour of the system repair during the service, and failure scenarios. However, most of these analyses are based on an individual PO and specific PIP materials. Interestingly, these studies highlighted that the loading conditions and the PIP material properties, in addition to environmental conditions, are critical factors affecting pipe failure mechanisms. There is a need, therefore, to define and design appropriately the PIP repair system with a range of mechanical properties under different loading conditions and failure modes.

This study characterizes POs through analytical and numerical modelling for a detailed understanding of the overall behavior of PIP systems. Initial screening models were implemented to satisfactorily investigate the effect of material and geometric properties of PIP systems to enable technology developers and the gas industry to establish the performance criteria for pipe replacement technologies. This study also develops design nomographs for PIP systems for a range of thicknesses and mechanical properties for different POs. The developed predictive modelling techniques and design tools for PIP systems will help in new material systems development and/or evaluation of their suitability for use as competent repair methods. These new design techniques can provide engineers and utilities with sufficient foundational guidance and necessary tools to begin exploring PIP for pipeline repair. Moreover, the Analytic hierarchy process (AHP) has been implemented to rank the POs and associated FMs. This new knowledge will also help improve the understanding of PIP systems for their uptake and exploitation in enhancing the performance and longevity of existing natural gas pipeline infrastructure, and may be adopted by other industries.

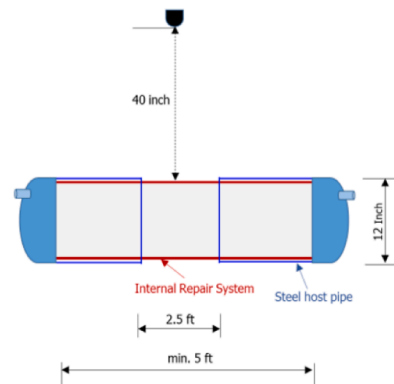
2. Modelling performance objectives of PIP systems

In this study, various POs, and potential FMs, of PIP systems were translated into predictive models to estimate the required material properties and thicknesses. This study also presents a framework to illustrate the procedure that can be followed to establish fundamental material performance (stiffness) and geometric characteristics (thickness) of PIP materials that are necessary to meet performance objectives. Finite element simulations and analytical modelling efforts were focused on assessing the structural performance of PIP systems under different load actions that will cause the POs, including (1) internal and external pressure including hydrostatic pressure, impact, etc., (2) vibration/fatigue due to traffic loads, (3) axial stresses and thermal deformation, and (4) bending moment and deformation during adjacent excavations and other ground movements. The selection of the POs is based on the current literature review, wherein most of the studies that evaluated the structural performance of the different PIP repair systems were conducted under internal pressure, bending moments, vibration and impact, and deformations (axial and transverse). The FE models for these POs were implemented using the following design parameters.

- **PO1:** Cyclic in-service surface loads or repetitive vibrational loads, due to overhead traffic, which may cause fatigue failure. The amount of rotation imposed on a buried cast iron pipeline with a circumferential crack that has been retrofitted with a Sanexen AP2/ALTRA repair decreases with the width of the crack. When the crack is 152.4 mm (6 in.) wide, the rotation is approximately 0.1°; it is estimated that in a 762-1016-762 mm (30-40-30 in.) 4-pt bending setup the load required to achieve this rotation is approximately 4.9 kN (1.1 kips). When the crack is 12.7 mm (0.5 in.) wide, the rotation is approximately 0.06°; it is estimated that in a 762-1016-762 mm (30-40-30 in.) 4-pt bending setup the load required to achieve this rotation is approximately 17.35 kN (3.90 kips). A crack width of 12.7 mm (0.5 in.) is representative of a joint that has lost significant rotational stiffness due to pullout. Hence, this force 17.35 kN (3.90 kips) has been used to determine the minimum thickness of the PIP system for each elastic modulus under the vibrational loading to achieve the design number of cycles at 1 million to reflect 50 years of service life [32].
- **PO2:** Deflection (lateral deformation), due to adjacent excavation, undermining, frost heave, ground subsidence, surface loads, or other sources. A design load of 178 kN (40 kips) is used to determine the minimum thickness of the PIP against deflection (lateral deformation). This level of load is based on the wheel loads positioned directly over a pipe and traveling parallel to the pipeline longitudinal axis and will generate stresses and deformations representative of worst conditions as found by Jeon et al. [19] and Stewart et al. [32].
- **PO3:** Cross-section ovalization may be due to external pressure, surface load, deflection (bending) of the pipeline and may be critical for low modulus PIPs and high buried depth (D)/ pipes thickness (t) ratio, e.g., culverts. Failure modes under cross-section ovalization were evaluated through parallel-plate loading following the test procedure described in ASTM D2412 [33] Standard Test Method for Determination of External Loading Characteristics of Plastic Pipe by Parallel-Plate Loading to identify critical properties of PIP repair systems for natural gas pipelines. The load capacity, stress, and strain of PIP at 5% and 10% diametric deflection is used to determine the minimum thickness for each elastic modulus under cross-section ovalization [33] where diametric deflection is the relative deflection of the PIP system with respect to its initial outer diameter. Moreover, the nonlinear behaviour of steel and cast-iron PIP is investigated based on available stress–strain curves for API X42 steel [34] and cast iron [35].
- **PO4:** Axial deformation (axial displacement), due to thermal expansion/contraction caused by seasonal temperature changes. Failure modes under axial deformation of the PIP due to thermal expansion/contraction by considering the seasonal temperature variation in the ground, which is applied incrementally by 5 °C (9 °F) were evaluated. The thermal coefficient of expansion of the PIP materials are approximated based on the relationship curve established from the review of the thermal coefficient of expansion of available materials with different elastic moduli [36].
- **PO5:** Circumferential (hoop) stress due to internal pressure and pressure fluctuations. Failure occurs when the internal pressure exceeds the short- and long-term stress carrying capacity of the host pipe-PIP system, excessive hoop stress in PIP with fully deteriorated host pipe. The circumferential (hoop) stress and strain experienced by the PIP with different thicknesses and ranges of modulus were evaluated under internal pressure of 60 psi, 100 psi and 200 psi. These pressures are representative of cast iron gas distribution mains that operate at less than 35 psi (~2 bar) pressure, as well as bare steel pipelines that operate at or below ~200 psi (~14 bar) pressure.
- **PO6:** Puncture of pipe system due to drop weight, rock impingement, host pipe fracture, contact by excavation equipment or other construction/external damage. The threat may result in dent, material loss, or crack, and thereby, loss or reduction of the system’s pressure carrying capacity. The model for the FE analysis to investigate the performance of the PIP under impact loading is developed based on the testing set-up and system reported in [37]. Dent, material loss or crack under impact loading caused by 1.5



(a) Lateral loading at CU Boulder



(b) Impact testing developed by GTI

Fig. 1. Experimental test set-up for PIP systems.

in (38.1 mm) semi-spherical drop weight of 1.1 lb (0.5 kg) at a height of 40 in. (1.016 m), referenced from the top of PIP. The weight is horizontally placed in the middle of the PIP as shown in Fig. 1(b).

2.1. Details of the FE model

Three-dimensional (3D) finite element (FE) models were developed either using ABAQUS/CAE standard FE software [38] or ANSYS/Mechanical FEA software [39] to establish the initial range of material properties and thicknesses of the PIP technologies suitable for natural gas pipelines and under the loading actions that correspond to POs 1–6. As the work presented is an outcome of the collaborative work between institutions wherein several researchers are working as a team to complete the analyses, ABAQUS/CAE standard FE software [38] has been used to investigate the POs 2–5 while ANSYS/Mechanical FEA software [39] has been used to investigate the PO1 and PO6. The FE model of POs are developed based on the experimental setup implemented by the University of Colorado Boulder for lateral loading and by the Gas Technology Institute in Chicago for impact [37] as shown in Figs. 1(a) and (b), respectively.

The FE models for the different failure modes were implemented for a PIP system with outer diameter conforming to the inner diameter of the host pipe [nominal 12-in. (300-mm) cast iron pipe – approximate outer diameter of 335 mm (13.2 in.) and wall thickness 14 mm (0.54 in.)]. The analyses focused on 300 mm (12 in.) diameter PIP systems as there are approximately 32000 km (20000 miles) of cast iron mains that exists based on the Pipeline and Hazardous Materials Safety Administration (PHMSA) database [40]. Lu et al. [6] also highlighted those pipelines with a diameter of 300 mm (12 in.) and smaller are expected to remain the main object of trenchless repair. The developed FE approach, however, can be extended to other diameters for cast iron and bare steel pipes. In the FE modeling, the maximum thickness of the PIP was limited to 25.4 mm (1 in.) because a higher thickness may not be cost effective and may affect the flow capacity of the repaired pipe. The wall thickness varied in an inward direction from 3.175 mm (0.125 in.) to 25.4 mm (1 in.) with increments of 3.175 mm (0.125 in.). The contribution of the existing host pipes was not considered as the PIP systems are anticipated not to rely on the external pipe to meet the 50-year service requirements. Examples of these FE models for POs are provided in Fig. 2. In all simulations, a mesh convergence study was carried out to ensure the accuracy and efficiency of the FE model. The stresses and strains caused by loads to induce the different FMs were analyzed to determine the required thickness and elastic modulus of the PIP systems.

The PIP system is modelled using 8-node 3-D solid element (C3D8R) with reduced integration and hourglass control for Abaqus and standard SOLID element for Ansys. In most cases, a detailed mesh at the most critical region was implemented. All the FE models were designed by confirming the replication of the physical experimental setup. The FE model for the PIP system has the following attributes:

- (1) nominal 307.8 mm (12.12 in.) outside diameter,
- (2) Modulus of Elasticity (MOE) of 1 GPa (145 ksi) to 200 GPa (29,008 ksi),
- (3) Thickness of 3.175 mm (1/8 in.) to 25.4 mm (1 in.) with increments of 3.175 mm (1/8 in.),
- (4) Isotropic material properties, and
- (5) linear elastic up to allowable strain (assumed failure).

For simplification, the quarter symmetry conditions are applied in longitudinal and transverse directions wherever possible. Pinned supports are used at both ends while the loading heads are connected with the pipe clamps via pin – lug system. Frictionless condition is used where contact happens between the PIP and the supports. The FE model for the PIP systems considered isotropic material properties and linear-elastic PIP material behavior up to the prescribed allowable strain limit.

2.2. PIP materials system

PIP systems with different material properties were considered in the analysis. Three general materials [steel, cast iron and glass fibre reinforced polymers (GFRP)] were considered in the investigation. In addition, 4 generic PIP materials with elastic modulus of 15

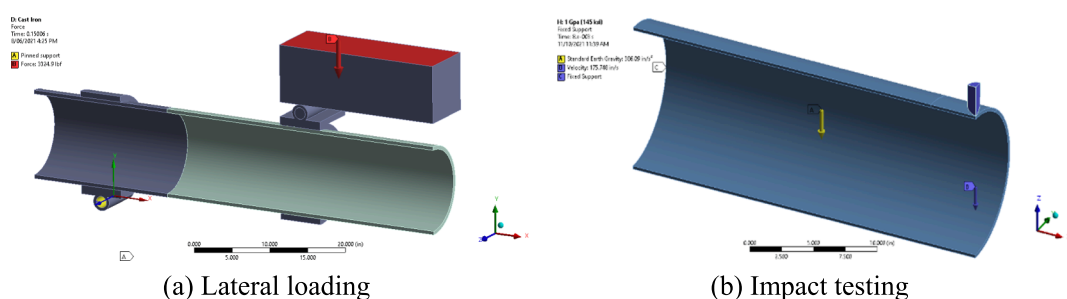


Fig. 2. FE models for modelling failure modes of PIP systems.

GPa (2176 ksi), 10 GPa (1450 ksi), 5 GPa (725 ksi) and 1 GPa (145 ksi) were investigated to provide a wide range of materials (i.e., unreinforced polymers, fiber reinforced thermosets and thermoplastics polymers, steel/polymer hybrid layers, particulate-filled polymers) that are intended to be representative of potential PIP material systems as shown in Table 1. Based on the initial material properties of the 24 internal repair technologies reported in Sirimanna et al. [14], the design strain for the analysis of the PIP systems was divided into two, i.e. 0.002 for metallic systems (70 GPa or 10,153 ksi or higher) and 0.02 for polymeric systems including composites and thermoplastics (24.5 GPa or 3553 ksi or lower). These design strain simplifications are based on the approximate yield strain of metallic and polymeric PIP material systems, respectively.

For modelling PO1 (vibrational load or fatigue), the S-N data for the polymeric materials are attuned from the S-N curve presented in [41,42], based on the strain criteria of 0.02 and the referenced S-N reduction rate. Detailed results of the FE simulations of the different POs are provided in the next sections. In modelling the axial deformation due to thermal load, the coefficient of thermal expansion (CTE) of the different PIP materials systems was established from the literature [36] and the relationship between them was plotted to establish an equation that can be used to approximate the CTE for materials with a specific elastic modulus. Fig. 3 shows the equation of the curve, which can be used to calculate the thermal coefficient of expansion for the generic PIP material systems while Fig. 3b shows the boundary conditions used in the FE model.

The coefficient of thermal expansion can be estimated using Eq. (1), where α_T is the coefficient of expansion ($\times 10^{-6}$ m/m °C) and E is elastic modulus (GPa).

$$\alpha_T = 70E^{-0.324} \tag{1}$$

2.3. Mesh convergence and calibration of the FE model

The mesh convergence study was carried out on the 25.4 mm (1 in.) thick and 1000 mm (39.4 in.) PIP under an internal pressure of 1.38 MPa (200 psi) to ensure the accuracy and efficiency of the FE model. The mesh convergence study results are shown in Table 2. Both length and width of the mesh were chosen as 5 mm based on previous mesh convergence studies [43–45]. The FE simulated hoop stress of PIP with the mesh size of $5 \times 5 \times 6.35$ mm was closest to the theoretical hoop stress (0.37% difference). Hence, in all FE models the mesh size was kept as close as possible of $5 \times 5 \times 6.35$ mm ($0.2 \times 0.2 \times 0.25$ in).

2.4. Validation of FE results

2.4.1. Lateral loading

The results of the FE analysis were validated by comparing with the theoretically predicted tensile stress results as shown in Table 3. Elastic section modulus of a circular hollow section,

$$S = \frac{\pi(D_e^4 - D_i^4)}{32D_e} \tag{2}$$

where D_e and D_i are the outer and inner diameters of the PIP, respectively.

The applied moment, $M = \frac{P}{2} \times x$, where P denoted the applied load and $x = 762$ mm (30 in.) gives theoretical stress of $\sigma_{theo} = \frac{M}{S}$. The tensile stress at the bottom-most layer at midspan of PIP obtained from the FE models are closely matched with the theoretically predicted tensile stresses and with the coefficient of variation (COV) and the mean ratio is 0.003 and 0.96, respectively.

2.4.2. Internal pressure

Similarly, the FE model simulated results were validated by comparing with the theoretically predicted hoop or circumferential stress in the PIP as a result of internal pressure. The hoop or circumferential stress in the PIP as a result of internal pressure is calculated based on both thin and thick plate theories. Circumferential or hoop stress (σ_h) for a thin wall ($D_e/t > 20$) can be calculated using equation (3):

$$\sigma_h = \frac{PD_e}{2t} \tag{3}$$

where P is the internal pressure, t is the wall thickness, and D_e is the outside diameter of the PIP.

On the other hand, hoop stress (σ_h) varies across the pipe wall from a maximum value on the inner surface to a minimum value on the outer surface of the PIP. The hoop stress for thick pipes ($D_e/t < 20$) at the inner surface based on the Lamé equation when there will be no external pressure can be calculated using Eq. (4):

Table 1
Properties of PIP materials.

Elastic Modulus (GPa) [ksi]	(1) [145]	(2) [290]	(3) [345]	(5) [725]	(10) [1450]	(15) [2176]	(24.5) [3553]	(70) [10153]	(200) [29008]
Poisson's ratio	0.11	0.11	0.11	0.11	0.11	0.11	0.11	0.29	0.29
Properties	Generic	Generic	Generic	Generic	Generic	Generic	GFRP	Cast iron	Steel

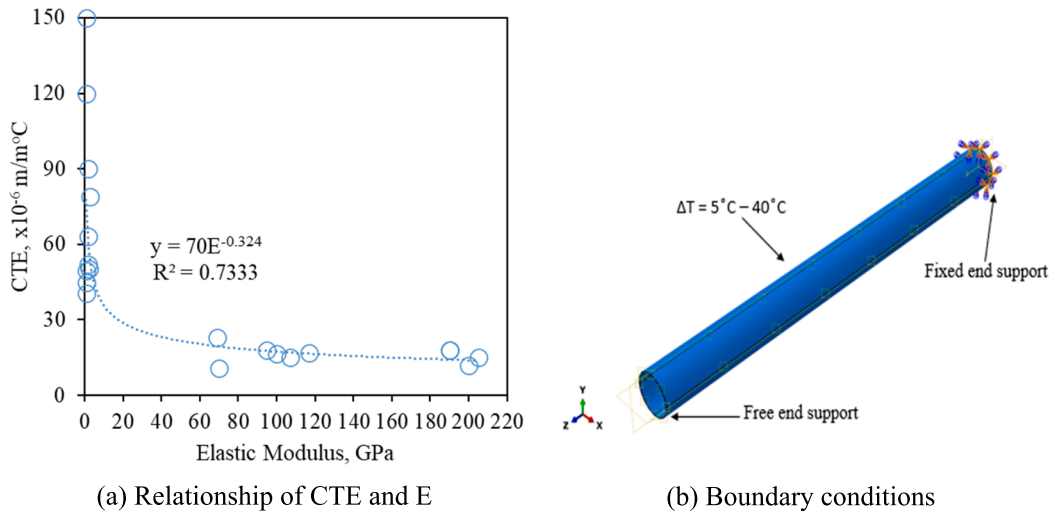


Fig. 3. Inputs for thermal load analysis.

Table 2
Mesh convergence study.

Mesh size (mm)	Element no	FE stress (MPa)	Theoretical stress (MPa)	% difference
5 × 5 × 6.35	152,800	7.7	7.73	0.37
5 × 5 × 8.47	114,600	7.63	7.73	1.28
5 × 5 × 12.7	76,400	7.52	7.73	2.70

Table 3
Comparison between theoretically and FE predicted tensile stress.

Modulus of elasticity (GPa)	Tensile stress (MPa)		FEM/theoretical
	Theoretical	FEM	
200.00	415.06	397.89	0.96
70.00	145.34	138.00	0.95
24.50	50.84	48.74	0.96
15.00	31.13	29.84	0.96
10.00	20.75	19.89	0.96
5.00	10.38	9.95	0.96
1.00	2.08	1.99	0.96
		Mean ratio	0.96
		COV	0.003

Table 4
Comparison between theoretically and FE predicted hoop stress.

Wall types	PIP thickness		Hoop stress (MPa)		FEM/theoretical
	mm	in.	Theoretical	FEM	
Thin wall	3.175	0.125	66.169	69.670	1.05
	6.35	0.25	32.751	33.361	1.02
	9.525	0.375	21.616	21.646	1.00
	12.7	0.5	16.053	15.473	0.96
Thick wall	15.875	0.625	12.718	12.497	0.98
	19.05	0.75	10.498	9.650	0.92
	22.225	0.875	8.914	8.743	0.98
	25.4	1	7.729	7.447	0.96
				Mean ratio	0.99
			COV	0.04	

$$\sigma_h = \frac{p_i(D_i^2 + D_e^2)}{D_e^2 - D_i^2} \tag{4}$$

where

- σ_h : Lamé hoop stress;
- D_e : external pipe diameter;
- D_i : internal pipe diameter and
- p_i : internal pressure of pipe.

The comparison between theoretically and FE predicted hoop stress is shown in Table 4. The hoop stresses obtained from the FE models closely matched the theoretically predicted hoop stresses, as indicated by the COV and the mean ratio are 0.04 and 0.99, respectively.

3. Results and discussion

The results of the FE analysis of the POs were validated with theoretical equations to confirm the reliability of the results. It is to be noted that the factor of safety and the projected 50-year properties of the PIP systems were not accounted for in the analysis.

3.1. PO1. Vibrational load

The fatigue life of the PIP due to vibrational load is predicted by using the critical stress and its stress-life (S-N) curve. In particular, the maximum tensile stress at the bottom-most layer of the PIP is firstly calculated under static loading. It is then projected to the S-N curve of the material to define the stress at failure and the according life cycle. The calculation of the critical tensile stress using numerical or analytical approaches is validated as shown in Table 3. As an example, the numerical results for tensile stress at the middle section of the pipe are shown in Fig. 4. Using the typical S-N curve for the PIP materials, the minimum life of the repair system is determined up to over 10 million cycles.

Fig. 5 shows calculated maximum stresses at the bottom most point of the PIP for different thicknesses. Tables 5 and 6 show maximum strain and displacement for different thicknesses and material properties. Based on the S-N curves of corresponding materials, Table 6 shows minimum cycles to failure of the PIP for various thicknesses and properties. From Tables 5 and 6, it is seen that when the maximum strain of the polymeric PIP system exceeds 0.02, the PIP fails to achieve its first cycle of loading. It requires a minimum thickness of 9.525 mm (0.375 in.) for MOE of 1 GPa (145 ksi) material to achieve 1 million cycles. While it only requires the minimum thickness of 3.175 mm (0.125 in) for MOE of 3 GPa (345 ksi) material to reach the design life. From the results, it is observed that the required thickness decreases with increasing MOE for polymeric PIP liners. PIP systems with an MOE of 70 GPa (10,153 ksi) require a minimum of 3.175 mm (0.125 in) thickness to achieve the target fatigue life cycle of 1 million.

3.2. PO2. Lateral deformation

FE simulations were implemented to investigate the performance of PIPs under lateral loading/bending with a range of MOE. Similarly, the load and the level of strain measured for PIP systems with different thicknesses under the lateral load of 178 kN (40 kips) were determined. The load capacity has been obtained for PIPs with different thicknesses at the strain of 0.002 and 0.02. The

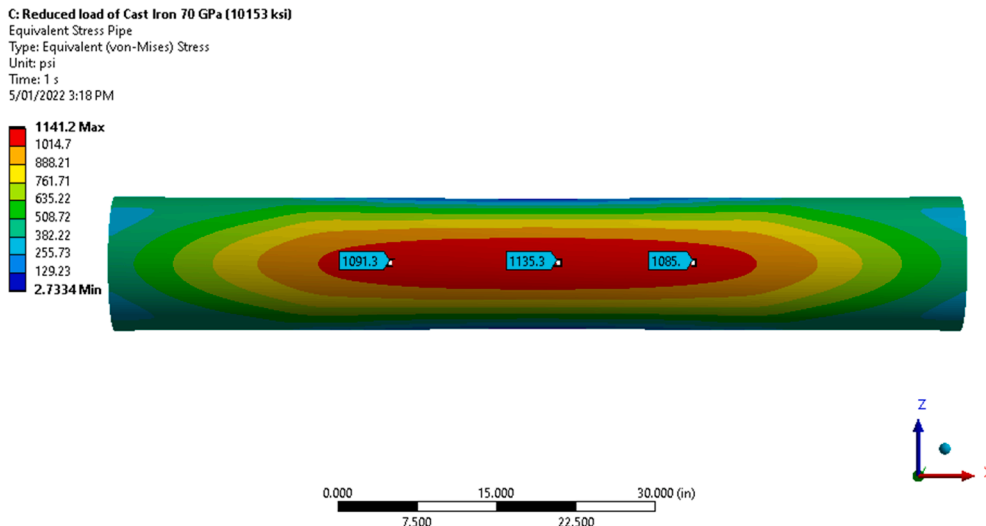


Fig. 4. Stress at cast iron PIP of 12.7 mm (0.5 in.) invert under vibrational load.

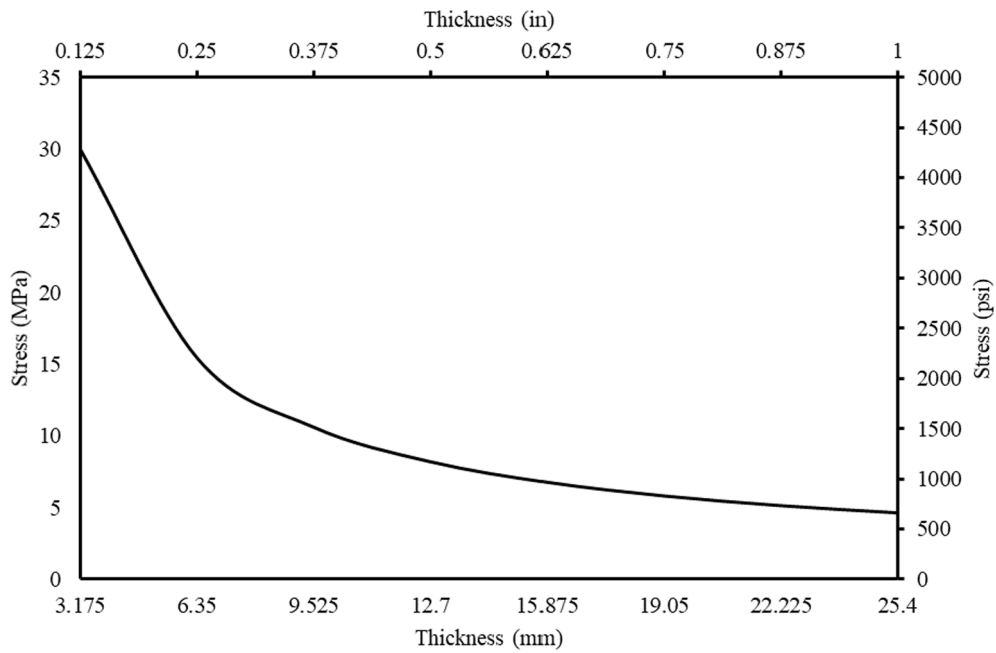


Fig. 5. Maximum stresses at the pipe invert for various pipe thicknesses.

Table 5

Maximum strain at the bottom-most point for various pipe thicknesses.

Thickness mm (in)	Maximum strain mm (in)								
	1 GPa (145 ksi)	2 GPa (290 ksi)	3 GPa (345 ksi)	5 GPa (725 ksi)	10 GPa (1450 ksi)	15 GPa (2176 ksi)	24.5 GPa (3553 ksi)	70 GPa (10153 ksi)	200 GPa (29008 ksi)
3.175 (0.125)	2.99E-02	1.44E-02	9.62E-03	5.77E-03	2.89E-03	1.92E-03	1.18E-03	4.12E-04	1.44E-04
6.35 (0.25)	1.54E-02	7.44E-03	4.96E-03	2.98E-03	1.49E-03	9.92E-04	6.08E-04	2.13E-04	7.44E-05
9.525 (0.375)	1.06E-02	5.12E-03	3.41E-03	2.05E-03	1.02E-03	6.83E-04	4.18E-04	1.46E-04	5.12E-05
12.7 (0.5)	8.22E-03	3.96E-03	2.64E-03	1.58E-03	7.92E-04	5.28E-04	3.23E-04	1.13E-04	3.96E-05
15.875 (0.625)	6.79E-03	3.27E-03	2.18E-03	1.31E-03	6.54E-04	4.36E-04	2.67E-04	9.34E-05	3.27E-05
19.05 (0.75)	5.83E-03	2.81E-03	1.87E-03	1.12E-03	5.62E-04	3.75E-04	2.30E-04	8.03E-05	2.81E-05
22.225 (0.875)	5.16E-03	2.49E-03	1.66E-03	9.95E-04	4.97E-04	3.32E-04	2.03E-04	7.11E-05	2.49E-05
25.4 (1)	4.66E-03	2.25E-03	1.50E-03	8.98E-04	4.49E-04	2.99E-04	1.83E-04	6.42E-05	2.25E-05

Table 6

Minimum life cycles to failure for various pipe thicknesses.

Thickness mm (in)	Number of cycles								
	1 GPa (145 ksi)	2 GPa (290 ksi)	3 GPa (345 ksi)	5 GPa (725 ksi)	10 GPa (1450 ksi)	15 GPa (2176 ksi)	24.5 GPa (3553 ksi)	70 GPa (10,153 ksi)	200 GPa (29,008 ksi)
3.175 (0.125)	0	2.6E + 04	1.7E + 08	1.9E + 11	3.7E + 13	2.1E + 14	8.2E + 14	» 1.00E + 07	» 2.00E + 07
6.35 (0.25)	4.1E + 03	9.0E + 09	8.3E + 11	3.1E + 13	4.7E + 14	1.2E + 15	2.3E + 15	» 1.00E + 07	» 2.00E + 07
9.525 (0.375)	2.7E + 07	6.2E + 11	1.4E + 13	1.7E + 14	1.1E + 15	2.0E + 15	3.3E + 15	» 1.00E + 07	» 2.00E + 07
12.7 (0.5)	2.2E + 09	5.1E + 12	5.7E + 13	3.9E + 14	1.7E + 15	2.7E + 15	3.9E + 15	» 1.00E + 07	» 2.00E + 07
15.875 (0.625)	3.0E + 10	1.8E + 13	1.3E + 14	6.5E + 14	2.1E + 15	3.2E + 15	4.3E + 15	» 1.00E + 07	» 2.00E + 07
19.05 (0.75)	1.7E + 11	4.2E + 13	2.3E + 14	9.1E + 14	2.5E + 15	3.6E + 15	4.6E + 15	» 1.00E + 07	» 2.00E + 07
22.225 (0.875)	5.8E + 11	7.6E + 13	3.4E + 14	1.2E + 15	2.9E + 15	3.9E + 15	4.8E + 15	» 1.00E + 07	» 2.00E + 07
25.4 (1)	1.4E + 12	1.2E + 14	4.6E + 14	1.4E + 15	3.1E + 15	4.1E + 15	5.0E + 15	» 1.00E + 07	» 2.00E + 07

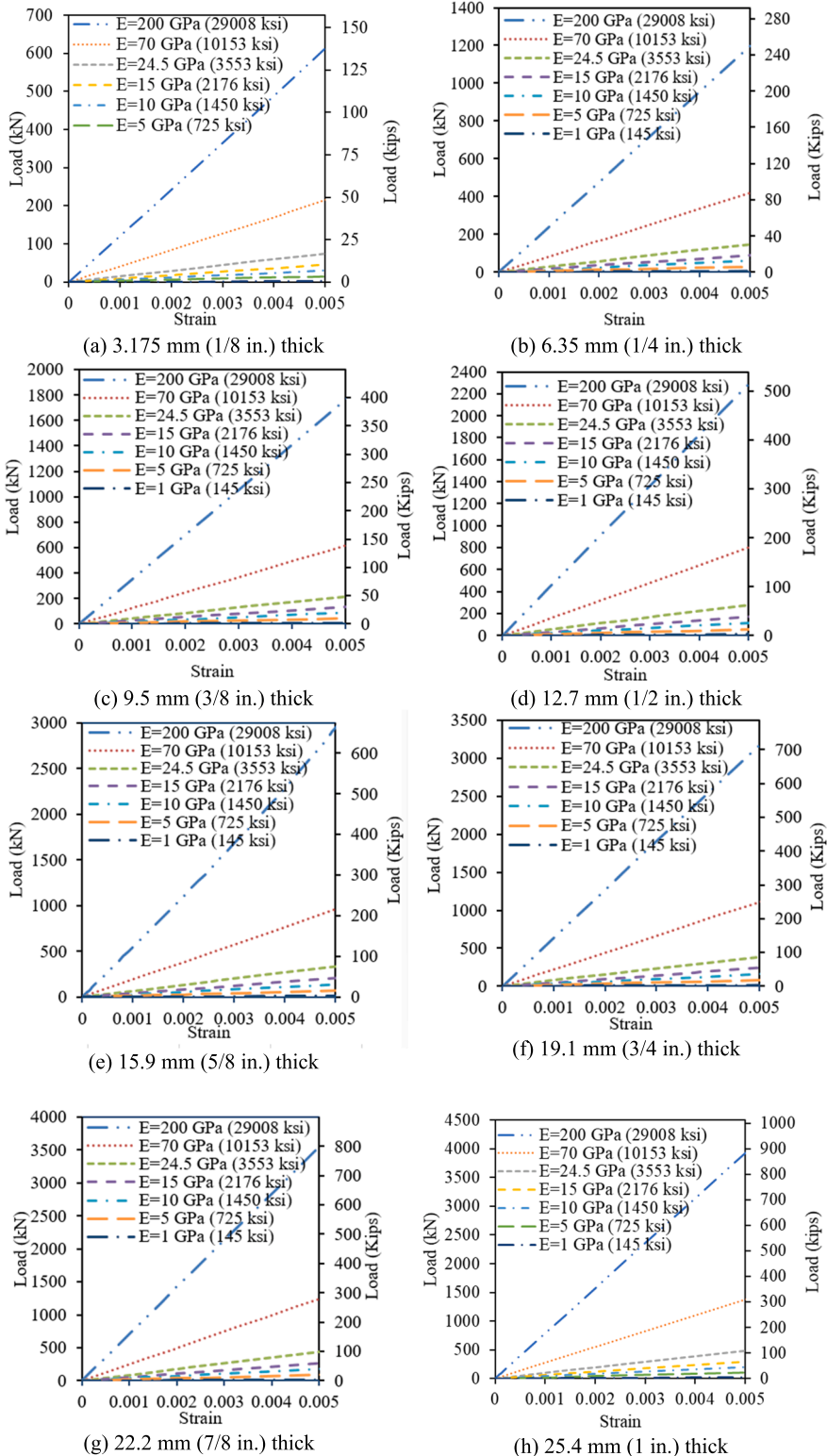


Fig. 6. Load-strain curves for PIP systems under lateral deformation.

load–strain curves for PIPs with thicknesses of 3.175 mm (1/8 in.)–25.4 mm (1 in.) and range of elastic modulus under bending are presented in Fig. 6.

The capacity of the polymeric PIP systems, i.e. 24.5 GPa (3553 ksi) and lower was evaluated at an elastic strain of 0.02. From the results, it was found the tensile strains in PIP systems with thickness of 9.5 mm (3/8 in.) and thinner does not reach at design strain of 0.02 due to the compressive non-linearity occurring at the compression zone (top of the PIP and between the loading points) as shown in Fig. 7. The maximum strain recorded is only 0.8%, 1.36%, and 1.76% strain for the PIP with a thickness of 1/8 in., 2/8 in., and 3/8 in., respectively. This failure behavior can be captured using nonlinear FE analyses considering the complete stress–strain behavior of the PIP material systems. Using the stress–strain behaviour of steel (MOE = 200 GPa or 29,008 ksi) reported in [34], a nonlinear FE analysis of a 3.175 mm (1/8 in.) thick PIP was implemented to verify the compressive buckling as shown in Fig. 8. For all moduli, the buckling failure can be eliminated when the thickness of the PIP is 12.7 mm (1/2 in.) or thicker.

The strain level of PIPs and composite PIPs with different thicknesses at the design lateral load of 178 kN (40 kips) is summarized in Figs. 9 and 10, respectively. Moreover, the lateral load capacity of PIPs and composite PIPs with different thicknesses at the design strain of 0.02 and 0.002 is summarized in Figs. 11 and 12, respectively. It is evident that the lateral load carrying capacity of the PIP with a higher modulus will be higher than those of a lower modulus. The summary of results in Figs. 9 and 11 show that a PIP with an MOE of at least 24.5 GPa (3553 ksi) is required to safely carry a lateral load of 40 kips when the strain is limited to 0.002, however, will need a thickness of at least 22.2 mm (7/8 in.). In addition, the summarized results for composite PIPs in Figs. 10 and 12 showed that a PIP system with an MOE of at least 5 GPa (725 ksi) and thickness of at least 12.7 mm (1/2 in.) is required to safely carry a lateral load of 40 kips when the strain is limited to 0.02. Moreover, the displacement at midspan as shown in Fig. 13 will be around 100 mm (4 in.) or a rotation of 7.5°. This may not be an issue for PIPs underground but may need consideration for polymeric PIP systems used aboveground.

3.3. PO3. Cross-section ovalization

Fig. 14 shows the stress diagram of the FE model through nonlinear FE analyses (MOE = 200 GPa or 29,008 ksi and $t = 25.4$ mm or 1 in.). The applied load–thickness curves for PIP with a range of elastic modulus under parallel-plate loading at 5% and 10% diametric deflection is shown in Figs. 15 and 16, respectively. It is evident that the lateral load carrying capacity of the PIP with higher thickness is higher than those with lower thickness. Moreover, at a certain lateral load capacity, the minimum thickness required to not exceed the 5% and 10% diametric deflection for the PIP with higher modulus is lower than those with lower modulus.

The diametric deflection (%) for PIP at design strain (0.002 for metallic PIP and 0.02 for composite PIP) is summarized in Table 7. The diametric deflection decreases with the increase of the thickness of PIP system while the lateral load capacity is increasing. The 3.175 mm (1/8 in.) thick steel and cast-iron PIP system can exhibit 16.2% and 15.6% diametric deflection, respectively, i.e. 50 mm (2 in.) and 48 mm (1.9 in.) lateral displacement, respectively. However, both steel and cast-iron PIP of 25.4 mm (1 in.) thick will have only 1.4% diametric deflection, i.e. 4.3 mm (0.17 in.) lateral displacement. On the other hand, all the 3.175–12.7 mm (1/8–1/2 in.) thick composites PIP system can have up to 32.5% diametric deflection, i.e. 100 mm (4 in.) lateral displacement but deform only 13.3% i.e. 41 mm (1.6 in.) lateral displacement when the thickness increases to 25.4 mm (1 in.). Moreover, the diametric deflection of the PIP with a lower modulus is higher than those with a higher modulus indicating that PIP with lower modulus has a higher tendency to fail due to cross-section ovalization.

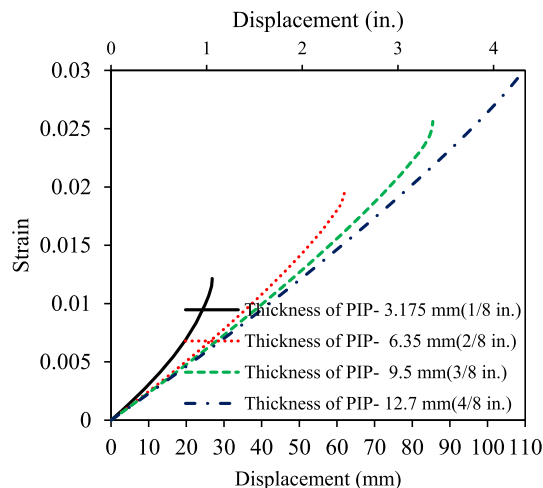


Fig. 7. Compressive strain–displacement curves for $E = 1$ GPa (145 ksi).

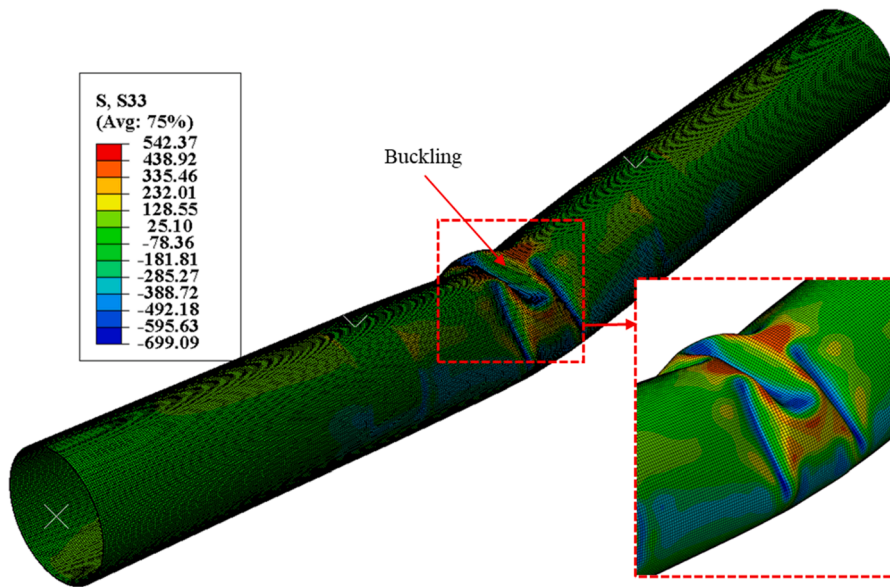


Fig. 8. Buckling of PIP systems under lateral deformation.

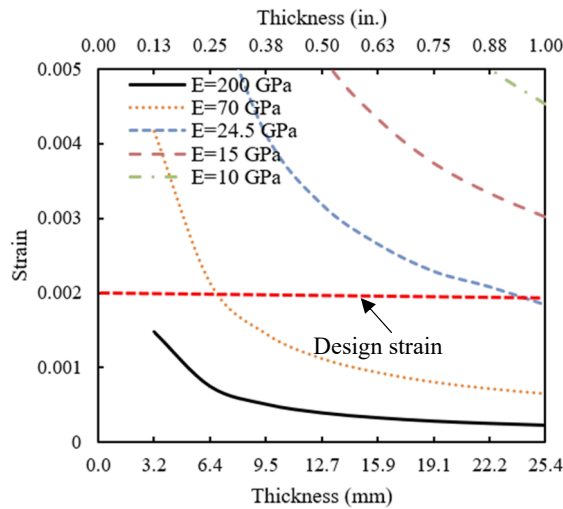


Fig. 9. Strain-thickness at 178 kN (40 kips) for metallic PIP.

3.4. PO4. Axial deformation due to thermal load

The seasonal temperature variation in the ground is applied incrementally by 5 °C (9 °F) to determine the level of the pipe elongation and stress and strain in the PIP system. The elongation (ΔL) of the PIP system with one end fixed and the other end free can be calculated using Eq. (5) and given below:

$$\Delta L = \alpha_T L \Delta T \tag{5}$$

where α_T is the coefficient of thermal expansion, L is the original PIP length, and ΔT is the difference between the final and initial service temperature of the PIP.

A study has been carried out analytically to investigate the effect of temperature change, (ranging between 5 °C (41°F) to 40 °C (104°F) with 5 °C increment) along with the types and thicknesses of PIP materials. Another boundary condition, which is both ends fixed, has been considered for all PIP materials and thicknesses. In the second boundary condition, an analytical calculation was carried out to determine the axial thermal forces of PIP due to changing in-service temperature and/or seasonal temperature within the same range evaluated in the first boundary condition. Fig. 17(a) shows the elongations of different PIP materials as a result of temperature change while Fig. 17(b) demonstrates the thermal loads against different thicknesses of PIP with E = 70 GPa (10,153 ksi) at

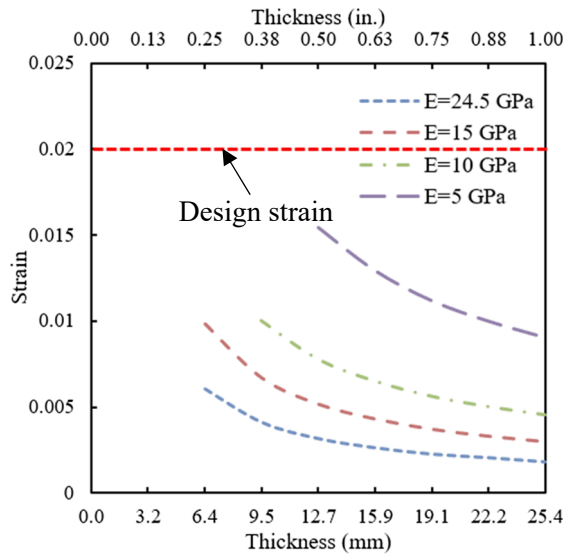


Fig. 10. Strain-thickness at 178 kN (40 kips) for composite PIP.

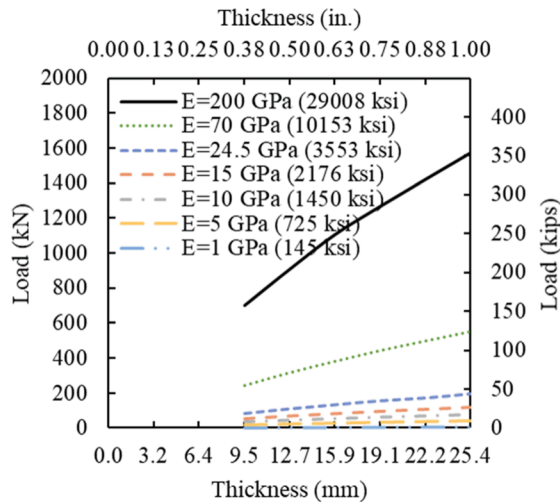


Fig. 11. Load-thickness at strain = 0.002 for PIP.

different temperatures. In the same way, thermal loads have been predicted for all PIP materials with the change in temperature. Furthermore, the level of temperature in which the PIP pipes will experience global buckling is estimated as shown in Fig. 19.

The seasonal temperature in New York State and other parts of the Northeast US fluctuate between 21 °C and -1 °C (70 °F and 30 °F) for the buried pipes at the typical depths [31,32] so the temperature increases by 22 °C (39.6 °F) from the winter season to the summer season is considered as a temperature change in the case study. PIP with different MOE (1 GPa (145 ksi) – 200 GPa (29008 ksi)) and pipe thickness (3.178 mm (1/8 in.)–25.4 mm (1 in.)) at $\Delta T = 22\text{ }^{\circ}\text{C}$ (39.6 °F) will elongate between 1.01 mm (0.04 in.) and 5.63 mm (0.22 in.). Based on 0.002 strain criteria for metallic PIP systems, the change in length (ΔL) of Cast Iron pipe with a length = 3657.6 mm (144 in.) is $0.002 \times 3657.6 = 7.31\text{ mm}$ (0.288 in.) and the same CI pipe length will elongate by 1.3 mm (0.05 in) at $\Delta T = 22\text{ }^{\circ}\text{C}$ (39.6 °F). The slenderness ratio (λ) of the PIP with different thicknesses (3.178 mm (1/8 in.)–25.4 mm (1 in.)) of the first boundary condition varies between 67.9 and 73. The slenderness ratio is calculated by dividing kL/r where k , L and r are the effective length constant depending on PIP ends boundary conditions, length of PIP, and radius of gyration, respectively. Therefore, all PIP materials and thicknesses will not buckle at the temperature change of 22 °C (39.6 °F) as can be seen in Fig. 18. This indicates that the current design parameter for axial deformation caused by thermal expansion may not be critical for the range of PIP systems considered in this study. Consideration should however be given to the change in material properties of PIP systems at any level of elevated in-service temperature. It is noted that the relatively flexible PIP system can bulge into the crack opening during cyclic thermal loading of high temperature change and can be pinched between host pipes, leading to failure. Moreover, the integrity of bond between the PIP and the host pipe with the temperature change should be considered in more detailed analysis of the PIP system.

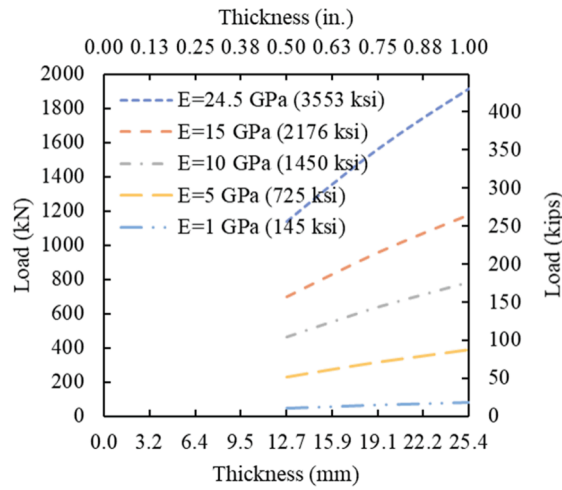


Fig. 12. Load-thickness at strain = 0.02 for composite PIP.

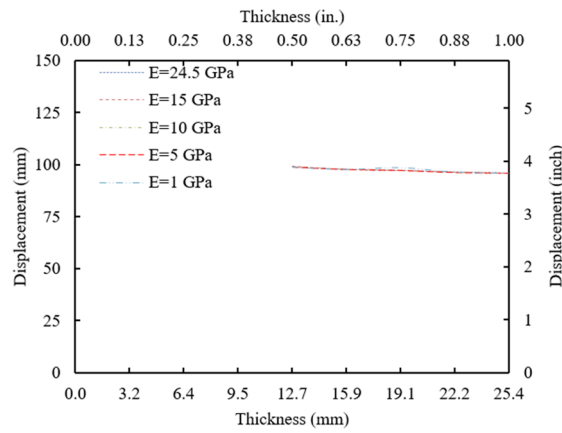


Fig. 13. Displacement-thickness at strain = 0.02 for composite PIP.

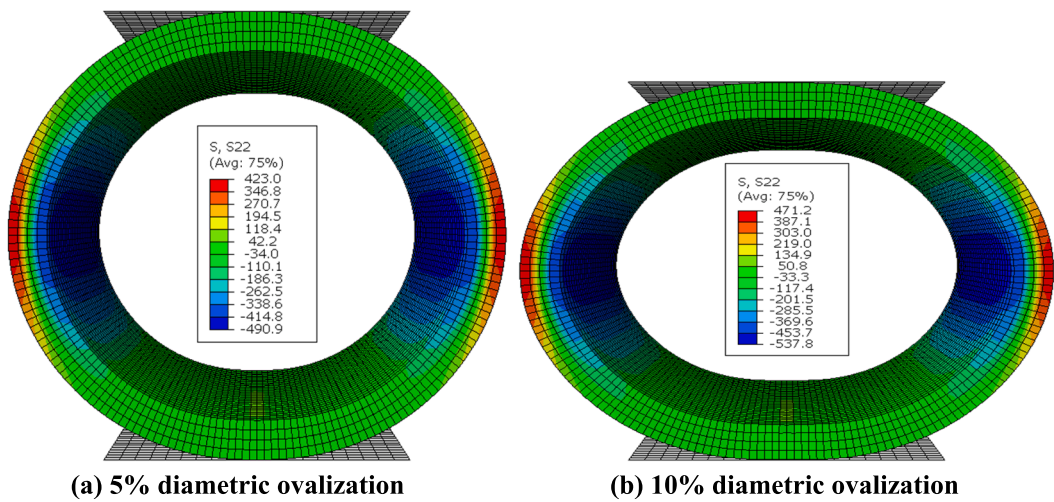


Fig. 14. Stress diagram of FE model through nonlinear FE analyses (MOE of 200 GPa (29,008 ksi) and thickness 25.4 mm (1 in.).

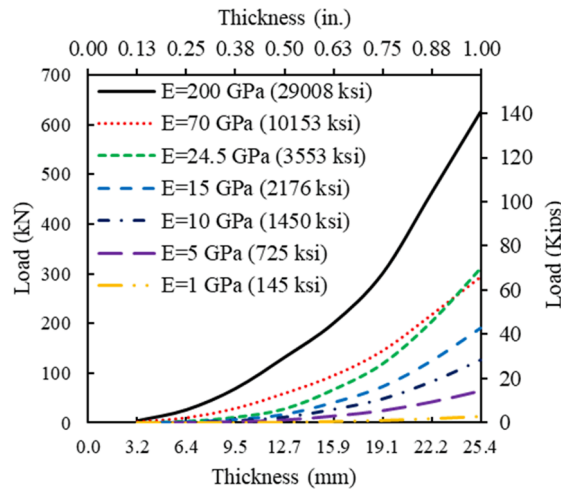


Fig. 15. Load-thickness curves at 5% diametric deflection.

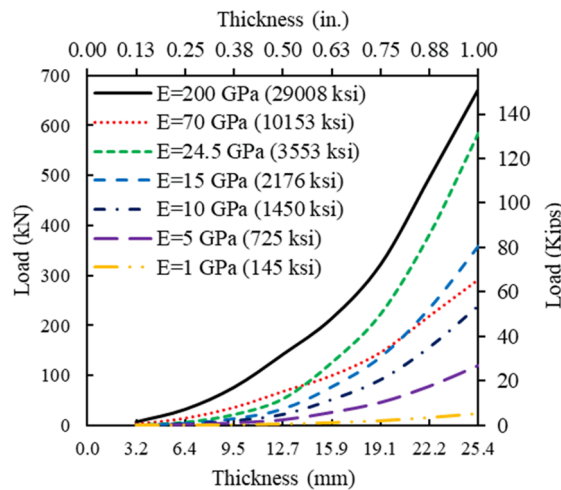


Fig. 16. Load-thickness curves at 10% diametric deflection.

Table 7

Percentage (%) diametric deflection for PIP system.

MOE GPa (ksi)	Thickness, mm (in.)							
	3.175 (1/8)	6.35 (2/8)	9.525 (3/8)	12.7 (1/2)	15.9 (5/8)	19.05 (6/8)	22.225 (7/8)	25.4 (1)
200 (29008)	16.2	8.3	5.7	4.5	2.4	2.1	1.6	1.4
70 (10153)	15.6	7.8	5.2	3.9	2.4	2	1.6	1.4
24.5 (3553)	32.5	32.5	32.5	32.5	23.7	19.7	15.1	13.3
15 (2176)	32.5	32.5	32.5	32.5	23.8	19.9	15.1	13.3
10 (1450)	32.5	32.5	32.5	32.5	23.7	19.7	15.1	13.3
5 (725)	32.5	32.5	32.5	32.5	23.8	19.7	15.1	13.3
1 (145)	32.5	32.5	32.5	32.5	23.9	19.7	15.1	13.3

3.5. PO5. Circumferential (Hoop) stress

The failure due to circumferential hoop stress of the PIP system was evaluated by applying internal pressure incrementally, and the level of strain and stress were noted. The length of the PIP was varied between 2 and 6 times of its outer diameter (D_e), i.e. $2D_e-6D_e$ to determine the minimum length of the FE model that will not be affected by the boundary conditions and will be developed almost uniform stress along the circumference and length of the PIP. The FE results show that the boundary support conditions have no significant effect on the stress and strain behavior of the PIP when the length of the pipeline is longer than $2 D_e$. Figure shows the

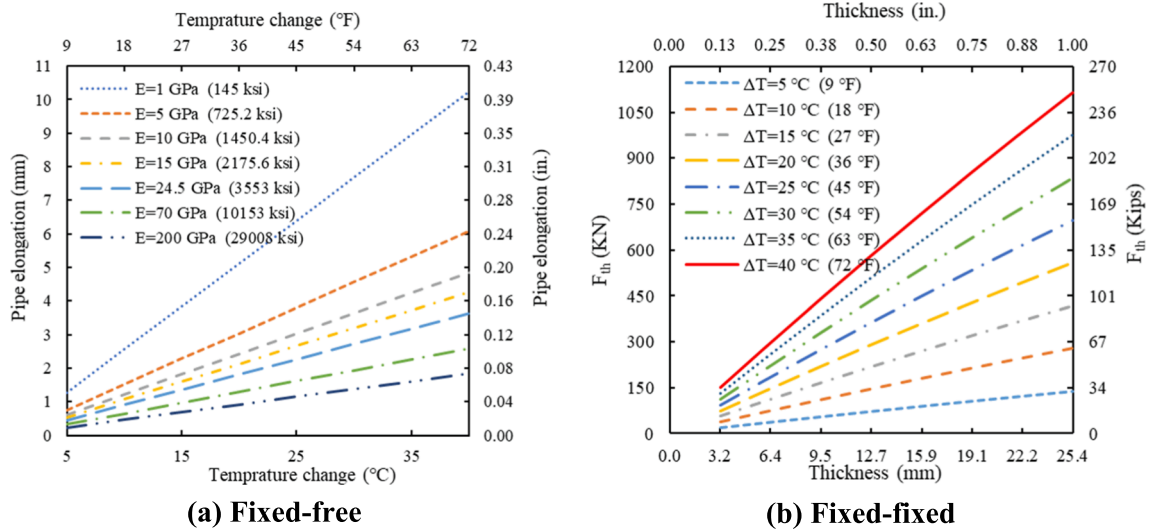


Fig. 17. (a) Pipe elongation and (b) thermal forces generated by different temperature changes for E = 70 GPa (10156 ksi).

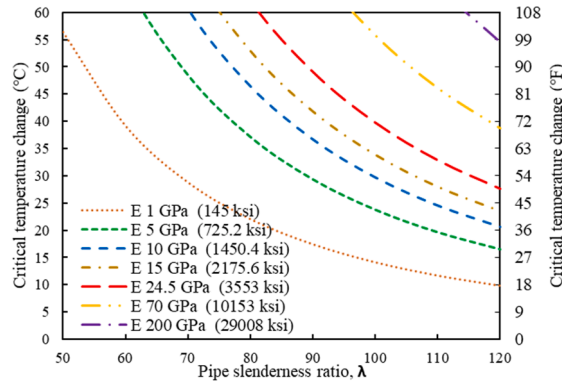


Fig. 18. Critical temperature change for different MOE.

minimum thickness required for PIP systems with a range of elastic modulus under internal pressure of 60, 100 and 200 psi based on a limiting strain of 0.002 along the hoop direction. A wall thickness exceeding 25.4 mm (1 in.) is required to resist the internal pressure for PIP materials with MOE of 1 GPa (145 ksi) at a maximum strain of 0.002. PIP materials, however, that have an MOE of 70 GPa (10,153 ksi) or higher just require a minimum wall thickness of 3.175 mm (1/8 in.) to resist the design internal pressure of 200 psi. The same minimum thickness can be achieved using PIP materials with a MOE of at least 15 GPa (2176 ksi) and 24.5 GPa (3553 ksi) to safely carry the design internal pressure of 60 psi and 100 psi, respectively. Fig. 19 shows the minimum thickness required for polymeric PIP technologies with MOE from 1 GPa to 24.5 GPa (145 ksi-3553 ksi) under internal pressure of 60, 100 and 200 psi based on a limiting strain of 0.02 along the hoop direction. It is important to note that a thickness of 3.175 mm (1/8 in.) is sufficient to resist the internal pressure of 60 psi for all ranges of moduli. Using 3.175 mm (1/8 in.) as the minimum thickness, the internal pressure of 100 psi and 200 psi can be safely resisted using PIP with a modulus of 5 GPa (725 ksi) or higher. The minimum required thickness will increase to 6.35 mm (1/4 in.) and 12.7 mm (1/2 in.) for 100 psi and 200 psi, respectively for a PIP with a modulus of 1 GPa (145 ksi). Please note however those design properties established from this analysis should consider the projected 50-year properties of the PIP technologies and apply an appropriate factor of safety based on the overall behavior of the materials.

3.6. PO6. Puncture of pipe system due to drop weight or external force

A 38.1 mm (1.5 in.) semi-spherical drop weight of 1.1 lb (0.5 kg) is used. It is freely dropped from a potential height of 1,016 mm (40 in.), referenced from the top of PIP. The weight is horizontally placed in the middle of the PIP as shown in Fig. 2 (b). For the sake of computational cost, the free-fall velocity at the time of impact was utilized and can be derived as follows.

$$V = \sqrt{2 \times g \times h} = 4.464 \frac{m}{s} \text{ or } 175.75 \frac{in}{s}$$

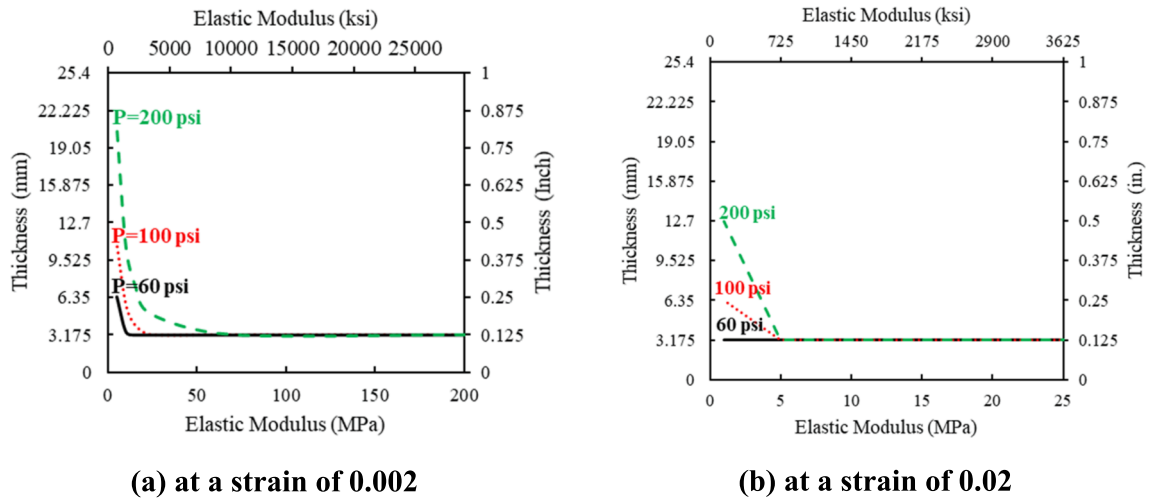


Fig. 19. Minimum thickness requirement for different design internal pressure.

where $g = 9.81 \frac{m}{s^2}$ ($32.17 \frac{ft}{s^2}$) is the standard acceleration due to earth gravity and $h = 1,016mm$ (40in.) is the drop height. The physical time of simulation ranges from 0.002 to 0.025 s until the drop weight, which was considered as a rigid body has completely given maximum impact effect onto the PIP systems in terms of damage and deformation.

Fig. 20 shows the meshing details of the model. At the impact region, an optimal mesh size of $2 \times 2 \times 2$ mm is used and a minimum of 5 elements are used in the thickness direction. For the rest of the model, the mesh sizes of 2.5×2.5 mm and 5×5 mm are used for the surfaces and 5 elements are used in the thickness direction. The mesh size of 2 mm is used for the rigid drop weight. The total number of elements used is ranging from 100,593 to 301,603 depending on the pipe thickness.

Fig. 21 shows the typical damage mode of PIP systems with different elastic moduli under impact loading. PIP systems with elastic modulus of 70 GPa (10,153 ksi) and 200 GPa (29,008 ksi) exhibited dent or damage caused by the limit exceeding strain in the impacted elements. For the thicknesses from 6.35 mm (0.25 in.) to 25.4 mm (1 in.), the drop weight typically makes an oval shape of dent or damage on the outermost surface of the PIP as shown in Fig. 21(a). However, for the thickness of 3.175 mm (0.125 in.) or lower, the damage happens on both outermost and innermost surfaces of the steel PIP. It penetrates through the thickness of the cast iron pipe as shown in Fig. 21(b). On the other hand, PIP systems with low elastic modulus, from 1 GPa (145 ksi) to 24.5 GPa (3553 ksi), over the range of thicknesses, deform under impact but gradually bounce back to its original shape. Typically, the 1 GPa (145 ksi) PIP at 3.175 mm (0.125 in.) is completely cracked along the longitudinal and circumferential lines under impact Fig. 21(b). However, at 6.35 mm (0.25 in.), the 1 GPa (145 ksi) PIP liner is damaged on the innermost surface due to exceeding the tensile strain.

Fig. 22 shows the maximum deflection under impact loading for different materials and thicknesses. PIP systems with an MOE of 1 GPa (145 ksi) have very high wall deflection, 44.112 mm (1.737 in.) and 8.881 mm (0.3496 in.), at 3.175 mm (0.125 in.) and 6.35 mm (0.25 in.) thicknesses, respectively. The resultant cracks are shown in Table 8. The high modulus materials of 70 GPa (10,153 ksi) yield 5.719 mm (0.225 in) deflection at 3.175 mm (0.125 in.) thickness, followed by the through wall thickness penetration as shown in Fig. 21(b). Figs. 23 and 24 show the maximum damage depth and its corresponding percentage for high modulus materials,

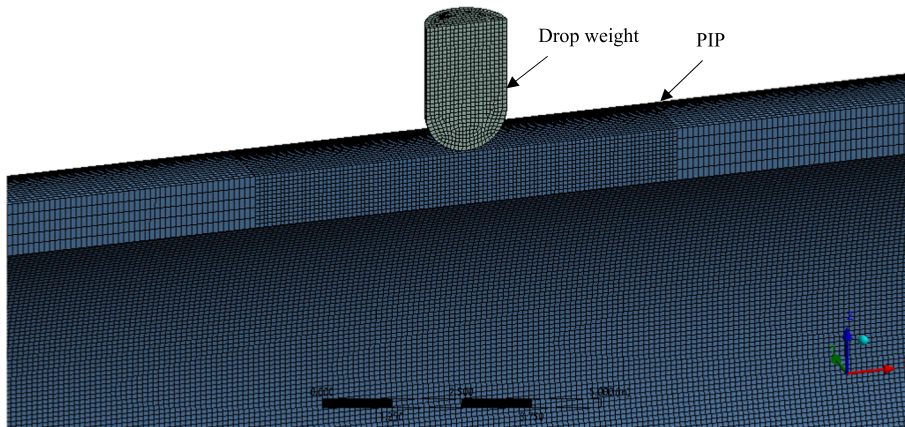
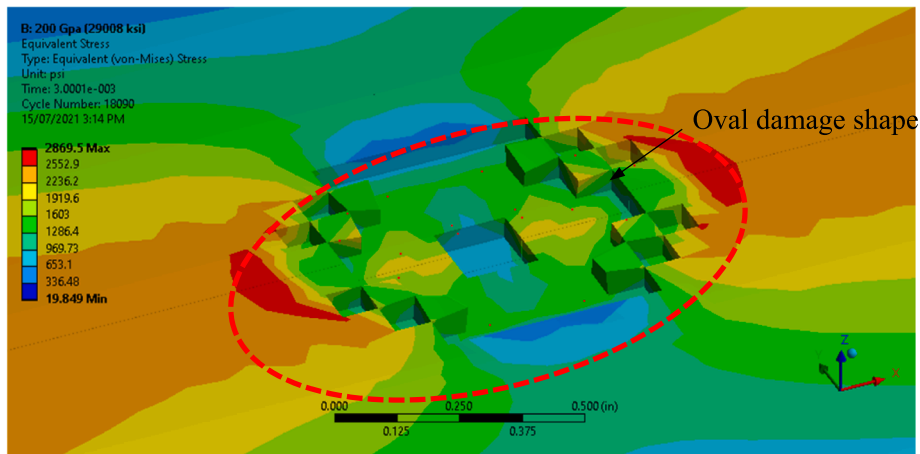
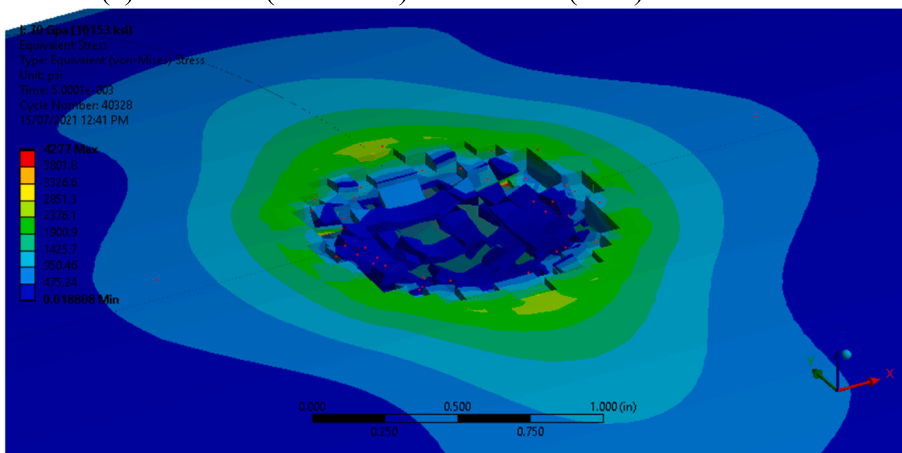


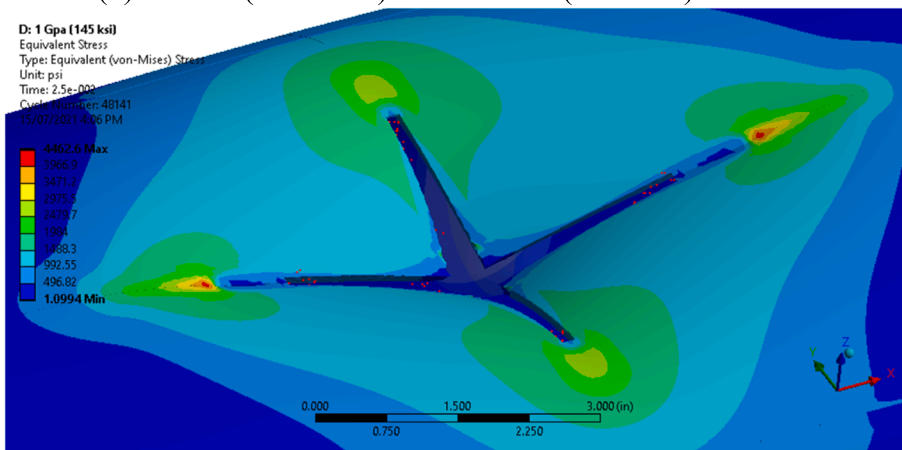
Fig. 20. Meshing of the model for the PIP of 25.4 mm (1 in) thick.



(a) 200 GPa (29008 ksi) at 25.4 mm (1 in.) thickness



(b) 70 GPa (10153 ksi) at 3.175 mm (0.125 in.) thickness



(c) 1 GPa (145 ksi) at 3.175 mm (0.125 in.)

Fig. 21. Typical failure modes of PIP system under impact.

respectively. If we set the percentage limit of 30% for the thickness damage (design factor of 3 for cast iron and 2 for steel), the minimum thickness requirement is 12.7 mm (0.5 in) for cast iron and 9.525 mm (0.375 in) for steel [46]. Figs. 25 and 26 show the damage sizes in longitudinal and circumferential directions for the high modulus materials. Overall, it can be observed that the drop weight produces larger damage on the cast iron surface.

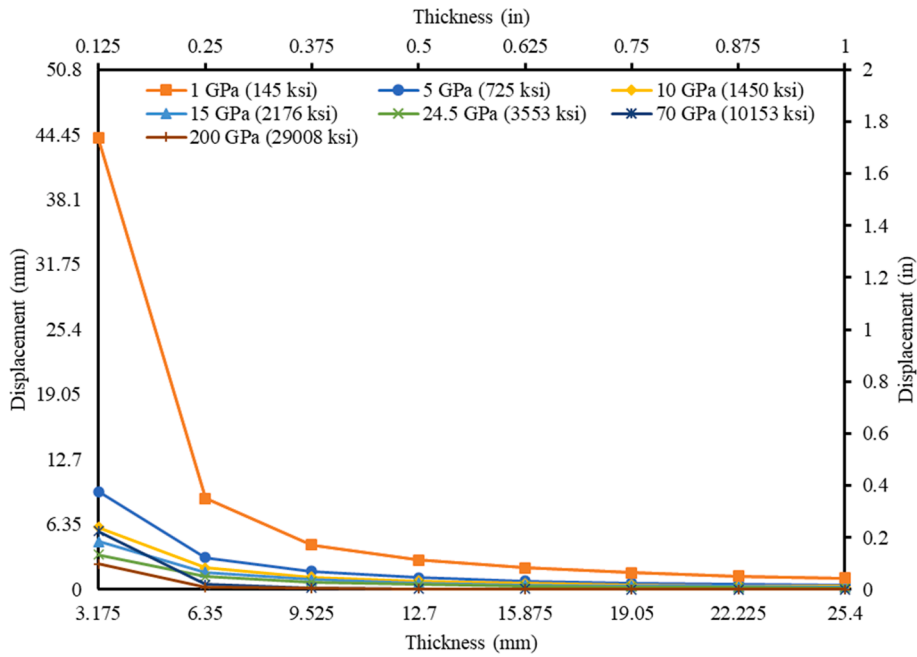


Fig. 22. Maximum deflection of PIP system under impact.

Table 8

Crack sizes in 1 GPa (145 ksi) material under impact.

MOE of 1 GPa (145 ksi)	PIP thickness (mm) [in.]	
	(3.175) [0.125]	(6.35) [0.25]
Crack depth (mm) [in.]	(3.175) [0.125]	(3.81) [0.15]
Percentage of damage depth	100%	60%
Crack length in longitudinal direction (mm) [in.]	(11.0) [4.33]	(41.91) [1.65]
Crack length in circumferential direction (mm) [in.]	(60.55) [2.3837]	(5.89) [0.2321]

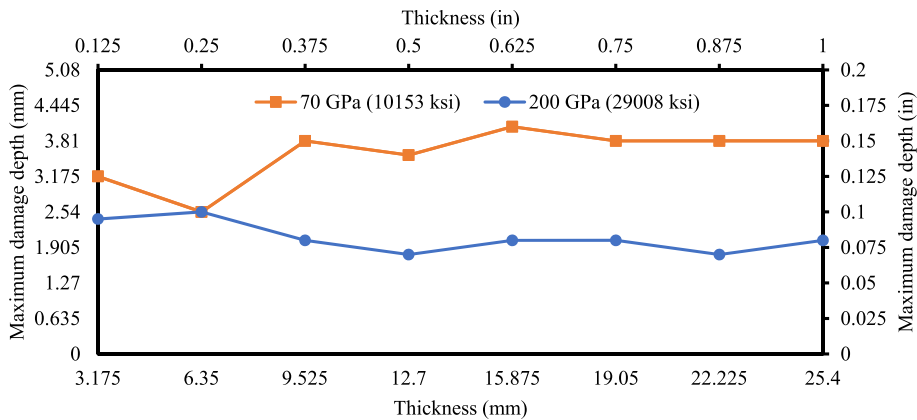


Fig. 23. Maximum damage depth at impact for high modulus materials.

4. Analytic hierarchy process (AHP) of failure modes

Analytic hierarchy process (AHP) was implemented to screen the identified failure modes for PIP systems for natural gas pipelines and supported by the results from FE simulations and theoretical analyses. The AHP can help identify the hierarchy of the critical performance objectives, identify the key design parameters that affect these failure modes including the critical mechanical properties of the repair system, and develop the most important testing techniques and protocols based on the level of importance. The AHP

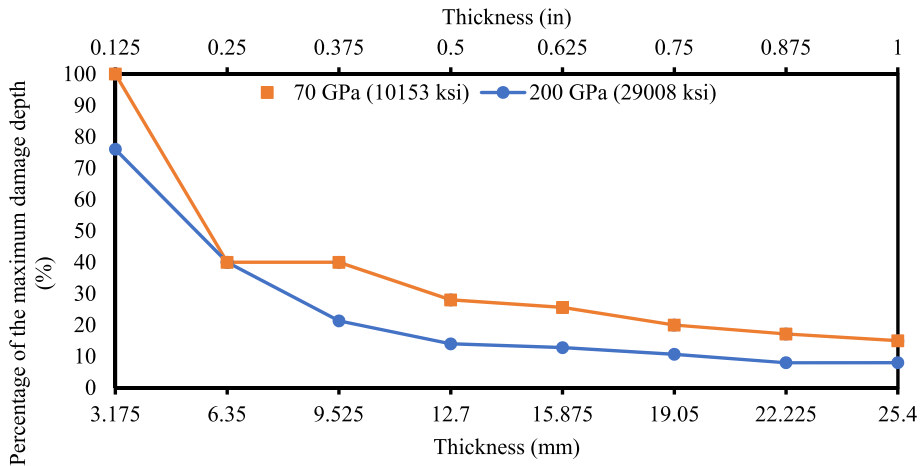


Fig. 24. Maximum damage percentage in depth for high modulus materials.

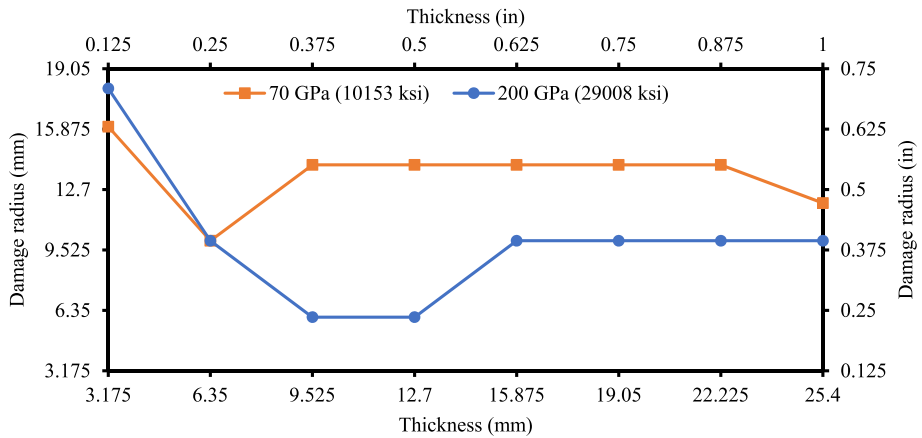


Fig. 25. Damage radius in the longitudinal direction for high modulus materials.

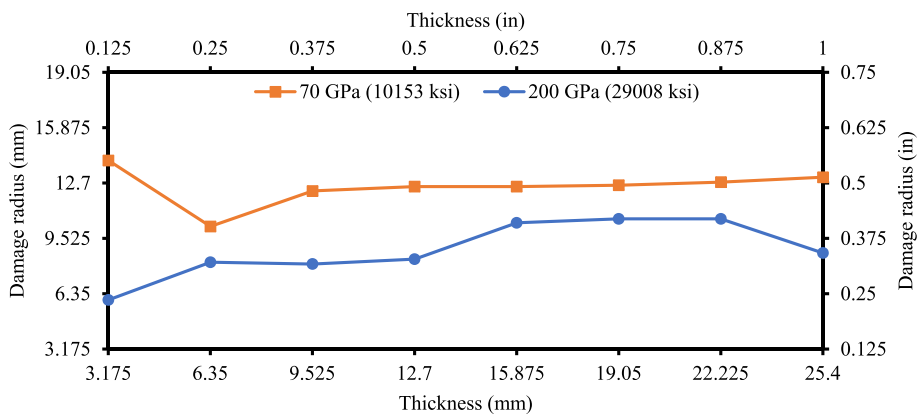


Fig. 26. Damage radius in the circumferential direction for high modulus materials.

proposed by Saaty and Vargas [47] provides measures of judgement consistency, derives priorities among criteria and alternatives, and simplifies preference ratings among decision criteria using pairwise comparisons [48]. It was applied successfully by Ferdous et al. [49] in the selection of the optimal mix of particulate-filled epoxy-based polymer coating and was used in this work to screen the identified performance objectives. The main advantage of this method over other multiple criteria decision-making methods is its

capability to check the consistency and reduce inconsistencies in judgement [47,49]. In addition, the AHP is scalable, easy to use, and big-sized decision problems can be accommodated easily by adjusting the hierarchy structure and less data-intensive method [50]. Moreover, this method has already been used in the pipeline industry as a decision support system in complex problems [51–53]. The outcome of the AHP is based on the attributes considered for each simulated PO as listed in Table 9. It is to be noted that the factor of safety and the projected 50-year properties of the PIP technologies were not accounted for in the analysis.

A relative importance matrix can be constructed for n attributes, where the relative importance of attribute i with respect to attribute j is represented by a_{ij} . An attribute is compared with itself in all the diagonal entries in the n -order square matrix. Hence, all of the diagonal entries in the n -order square matrix are equal to 1. For example, $a_{11} = a_{22} = a_{33} = \dots = a_{nn} = 1$.

A typical relative importance matrix $A = [a_{ij}]_{n \times n}$ can be expressed by Eq. (6) which has reciprocal properties where $a_{ji} = 1/a_{ij}$ and $a_{nn} = 1$.

$$A = \begin{bmatrix} a_{11} & \dots & a_{1n} \\ \vdots & \ddots & \vdots \\ 1/a_{1n} & \dots & a_{nn} \end{bmatrix} = \begin{bmatrix} 1 & \dots & a_{1n} \\ \vdots & \ddots & \vdots \\ 1/a_{1n} & \dots & 1 \end{bmatrix} \tag{6}$$

The normalized eigenvector of matrix A represents the relative weights of the attributes and is called the priority matrix. The eigenvector of matrix A can be determined manually or by using a computation tool (e.g., spreadsheet). The eigenvector is normalized by dividing an element of the eigenvector a_{ij} by the sum of all its elements, according to the expression in Eq. (7):

$$a_{ij}^* = \frac{a_{ij}}{\sum_{i=1}^n a_{ij}} \tag{7}$$

4.1. Relative intensities of criteria and alternatives

The criteria are the main drivers for selection of the critical failure mode. A small change in intensity of criteria and alternatives has a significant effect on the final output, and the priorities of the properties depend on the design requirements. The fundamental FE models developed and implemented in Section 3 focused on investigating the effect of the thickness and elastic modulus to determine the initial ranges for acceptable mechanical properties and thicknesses of the PIP. Hence, the thickness and modulus of elasticity of the PIP system have been chosen as the criteria and are given the same level of priority in the AHP process at this stage. Other important parameters can be considered as criteria in the AHP process based on more detailed information on the material and geometric properties. All the performance objectives (PO1-6) considered in the AHP are chosen as alternatives. The relative weightings of the alternative POs have been taken based on their performance.

The outcome parameters based on design internal pressures of 60 psi (414 kPa), 100 psi (690 kPa) and 200 psi (1379 kPa) are listed in Tables 10, 11 and 12, respectively. Those outcome parameters have been listed based on the results of detailed analysis in Section 3. The first column of the outcome parameters is for the thickness requirement for the minimum required modulus of elasticity for each performance objective. For example, the outcome parameters in the first column of Table 11 for PO5 and the design internal pressure of 100 psi (690 kPa) are chosen as 1/4 in. (6.35 mm) and 145 ksi (1 GPa) when the criteria is the thickness and elastic modulus, respectively. In other words, for a PIP with an elastic modulus of 145 ksi (1 GPa), a thickness of 1/4 in. (6.35 mm) is required to safely resist an internal pressure of 100 psi (690 kPa). The second column of the outcome parameters represents the modulus of elasticity requirement for the minimum required thickness for each PO. For example, the outcome parameters in the second column of Table 11 for PO5 and the design internal pressure of 100 psi (690 kPa) are chosen as 1/8 in. (3.175 mm) and 725 ksi (5 GPa) when the criteria is the thickness and elastic modulus, respectively. In this case, a minimum wall thickness of 1/8 in. (3.175 mm) is required to resist the design internal pressure of 100 psi (690 kPa) if the PIP materials have an elastic modulus of at least 725 ksi (5 GPa). However, the metallic PIP systems are more critical compared to composite PIP systems under PO6 (impact loading) which is the reverse behavior compared to all other FMs due to their high elastic moduli.

The relative weightings of the alternative POs were chosen based on the outcome parameters for the three design internal pressures and presented in Tables 10, 11 and 12, respectively. For example, when the AHP criteria is the thickness and the design internal pressure is considered as 60 psi (414 kPa), PO2 gives the highest relative weighting (10) as PO2 requires the thickest PIP, 1/2 in. (12.7 mm), for the minimum required modulus of elasticity, 725 ksi (5 GPa). Likewise, PO3 and PO5 will have the lowest relative weighting

Table 9
Attributes considered for simulated POs of PIP systems.

Notation	Attributes
PO1	Target life cycle of approximately one-half to one million cycles of repetitive deflections caused by repeated overhead traffic loads applied to a pavement and subgrade system equivalent to 3,900 lbf (17,350 N) based on a design displacement of approximately 0.07 in. (1.78 mm) for nominal 12-in. (300-mm) diameter cast iron pipe [19,32,54–56].
PO2	Pipeline deflections are caused by traffic loads applied to a pavement and subgrade system. Deflection (lateral deformation) under the design lateral load of 40 kips (178 kN) [19,32,54–56].
PO3	Cross-section ovalization up to 5% and 10% diametric deflection [33].
PO4	Axial deformation (axial displacement) due to thermal expansion/contraction at a temperature change of 22 °C (40 °F).
PO5	Circumferential (hoop) stress due to internal pressure of 60 psi (414 kPa), 100 psi (690 kPa) and 200 psi (1379 kPa).
PO6	Dent, metal loss or crack under impact loading caused by 1.5 in. (38.1 mm) semi-spherical drop weight of 1.1 lb (0.5 kg) at a height of 40 in. (1.02 m) [37].

Table 10
Relative weightings of alternative POs for design internal pressure of 60 psi (414 kPa).

	PO Criteria	Vibration loads		Lateral deformation		Cross-section ovalization		Axial deformation		Internal Pressure		Impact	
		PO1	PO2	PO3	PO4	PO5	PO6						
Outcome Parameter	Thickness (in.)	3/8	1/8	1/2	1/8	1/8	1/8	1/8	1/8	1/8	1/8	3/8	1/8
	Modulus of elasticity (ksi)	145	345	725	29,008	145	145	145	145	145	145	145	725
Relative weighting	Thickness	9		10		6		7		6		9	
	Modulus of elasticity	8		10		7		7		7		9	

Table 11
Relative weightings of alternative POs for design internal pressure of 100 psi (690 kPa).

	PO Criteria	Vibration loads		Lateral deformation		Cross-section ovalization		Axial deformation		Internal Pressure		Impact	
		PO1	PO2	PO3	PO4	PO5	PO6						
Outcome Parameter	Thickness (in.)	3/8	1/8	1/2	1/8	1/8	1/8	1/8	1/8	1/4	1/8	3/8	1/8
	Elastic of Modulus (ksi)	145	345	725	29,008	145	145	145	145	145	725	145	725
Relative weighting	Thickness	9		10		6		7		8		9	
	Modulus of elasticity	7		10		6		6		8		9	

Table 12
Relative weightings of alternative POs for design internal pressure of 200 psi (1379 kPa).

	PO Criteria	Vibration loads		Lateral deformation		Cross-section ovalization		Axial deformation		Internal Pressure		Impact	
		PO1	PO2	PO3	PO4	PO5	PO6						
Outcome Parameter	Thickness (in.)	3/8	1/8	1/2	1/8	1/8	1/8	1/8	1/8	1/2	1/8	3/8	1/8
	Elastic of Modulus (ksi)	145	345	725	29,008	145	145	145	145	145	725	145	725
Relative weighting	Thickness	8		10		6		7		9		8	
	Modulus of elasticity	8		10		7		7		9		9	

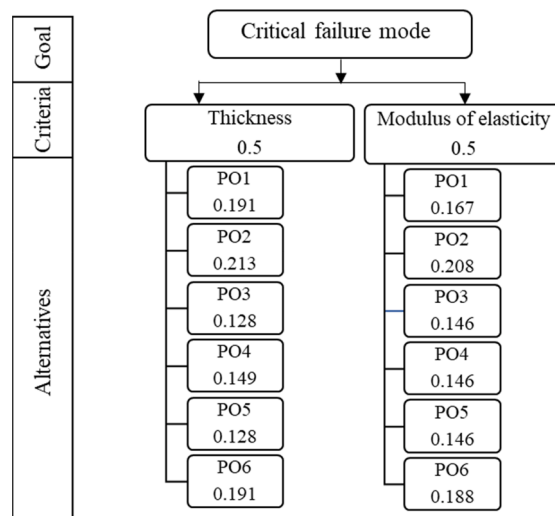


Fig. 27. The hierarchy of local priorities based on design pressure of 60 psi (414 kPa).

(6). In addition, PO2 gives the highest relative weighting (10) as it requires the highest modulus of elasticity, 29,008 ksi (200 GPa), for the minimum required thickness 1/8 in. (3.175 mm). Similarly, PO3, PO4 and PO5 have the lowest relative weighting (7) for the alternative case when the AHP criteria is the modulus of elasticity and the design internal pressure considered as 60 psi (414 kPa). It is noted that, while the highest relative weighting of 10 is given, a reduction of 1 is applied to the next criteria (a reduction of only 10%) to minimize bias between the different POs as the design criteria for each PO are different and the relative importance of these criteria against each other is difficult to establish.

4.2. Hierarchy of local priorities for critical POs for PIP system

In the present AHP, the pair-wise comparison matrix (relative importance matrix as per Eq. (6)) which holds the preference values has been obtained based on the relative weightings of the different alternatives. The matrix was then normalized following Eq. (7). The developed hierarchy to rate and compare the alternatives for each criterion for the design pressure of 60 psi (414 kPa), 100 psi (690 kPa) and 200 psi (1379 kPa) has been shown in Figs. 27, 28 and 29, respectively.

4.3. Ranking of critical POs for PIP system

The separate rankings of the critical POs for the PIP system have been developed based on the criteria (thickness and modulus of elasticity of PIP system) as well as global priority. The global priority of critical POs for the PIP system was determined by multiplying its corresponding local priorities and summing them together, and expressed as

$$\text{Global priority of critical POs} = \sum [Priority_{\text{alternative}} \times Priority_{\text{criteria}}] \tag{8}$$

The rankings of the critical POs for PIP systems when the design pressure of 60 psi (414 kPa), 100 psi (690 kPa) and 200 psi (1379 kPa) are presented in Tables 13, 14 and 15, respectively. It is evident that the PO2 (lateral deformation) is the most critical PO based on global priority as well as both criteria (thickness and modulus of elasticity of PIP system) for all the design pressure of 60 psi (414 kPa), 100 psi (690 kPa) and 200 psi (1379 kPa). PO6, PO1, PO4, PO5 and PO3 respectively are the global ranking for the rest of critical POs when the design pressure is considered as 60 psi (414 kPa). Moreover, the global ranking of the rest of critical failure modes for PIP systems is PO6, PO5, PO1, PO4 and PO3 respectively when the design pressure is considered as 100 psi (690 kPa) and PO5, PO6, PO1, PO4 and PO3 respectively when the design pressure is considered as 200 psi (1379 kPa). Hence, PO3 (cross-section ovalization) is found to be the least critical failure mode of the PIP system for any design internal pressure. It is important to note, however, that these rankings are based on the attributes considered for each simulated PO listed in Section 3. It is also noted that the factor of safety and the projected 50-year properties of the PIP technologies was not accounted for in the analysis.

5. Conclusion

Analytical and numerical modelling was implemented to investigate the effect of material and geometric properties on different POs for pipe-in-pipe (PIP) systems. Based on the results of the study, the following conclusions can be drawn:

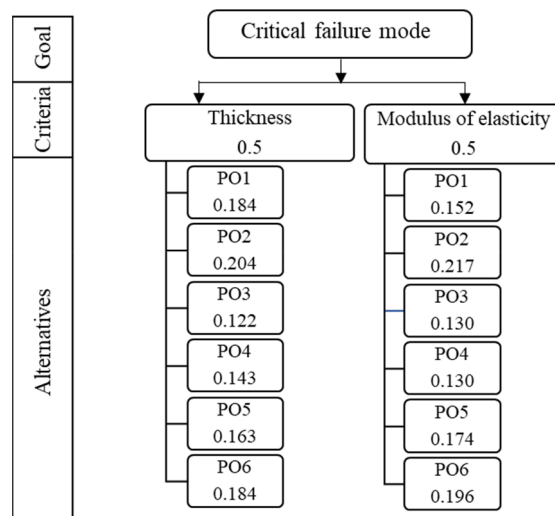


Fig. 28. The hierarchy of local priorities based on design pressure of 100 psi (690 kPa).

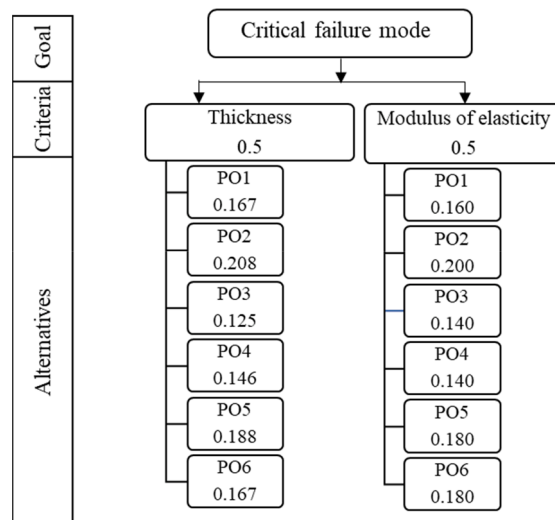


Fig. 29. The hierarchy of local priorities based on design pressure of 200 psi (1379 kPa).

Table 13
Ranking of critical PIP POs for design internal pressure of 60 psi (414 kPa).

Criteria						Global priority			
Thickness			Modulus of Elasticity						
Rank	PO	Priority (%)	Rank	PO	Priority (%)	Rank	PO	Priority (%)	
1	PO2	21.3	1	PO2	20.8	1	PO2	21.1	
2	PO6	19.1	2	PO6	16.7	2	PO6	18.9	
3	PO1	19.1	3	PO1	18.8	3	PO1	17.9	
4	PO4	14.9	4	PO5	14.6	4	PO4	14.7	
5	PO5	12.8	5	PO4	14.6	5	PO5	13.7	
6	PO3	12.8	6	PO3	14.6	6	PO3	13.7	

Table 14
Ranking of critical PIP failure modes for design internal pressure of 100 psi (690 kPa).

Criteria						Global priority			
Thickness			Modulus of Elasticity						
Rank	PO	Priority (%)	Rank	PO	Priority (%)	Rank	PO	Priority (%)	
1	PO2	20.4	1	PO2	21.7	1	PO2	21.1	
2	PO6	18.4	2	PO6	19.6	2	PO6	19.0	
3	PO1	18.4	3	PO5	17.4	3	PO5	16.9	
4	PO5	16.3	4	PO1	15.2	4	PO1	16.8	
5	PO4	14.3	5	PO4	13.0	5	PO4	13.7	
6	PO3	12.2	6	PO3	13.0	6	PO3	12.6	

Table 15
Ranking of critical PIP failure modes for design internal pressure of 200 psi (1379 kPa).

Criteria						Global priority			
Thickness			Modulus of Elasticity						
Rank	PO	Priority (%)	Rank	PO	Priority (%)	Rank	PO	Priority (%)	
1	PO2	20.8	1	PO2	0.200	1	PO2	20.4	
2	PO5	18.8	2	PO5	0.180	2	PO5	18.4	
3	PO6	16.7	3	PO6	0.180	3	PO6	17.3	
4	PO1	16.7	4	PO1	0.160	4	PO1	16.3	
5	PO4	14.6	5	PO4	0.140	5	PO4	14.3	
6	PO3	12.5	6	PO3	0.140	6	PO3	13.3	

- Target life cycle of 1 million under cyclic in-service surface loads caused by repeated overhead traffic loads can be achieved by PIP systems with an elastic modulus of at least 1 GPa (145 ksi) and thickness of 9.525 mm (3/8 in). The required thickness decreased with the increase in the elastic modulus of the PIP material systems.
- The lateral load carrying capacity of the PIP system increases with the increase in thickness and elastic modulus. PIP systems with a thickness of 9.525 mm (3/8 in.) or lower will experience compressive buckling before reaching a tensile strain of 0.02. Buckling failure can however be eliminated for PIP when the thickness is 12.7 mm (4/8 in.) or higher. PIP system with a modulus of at least 5 GPa (725 ksi) and thickness of 12.7 mm (4/8 in.) is required when the strain is limited to 0.02 while a modulus of at least 24.5 GPa (3553 ksi) and thickness of 22.225 mm (7/8 in.) is needed when the strain is limited to 0.002.
- The tendency for cross-section ovalization of the PIP system decreases with the increase in thickness and elastic modulus. Polymeric-based PIP materials can have a diametric deflection of up to 32.5% without reaching a strain of 0.02 while metallic-based PIP system will only deform by 16.2% at a strain of 0.002.
- Polymeric PIP systems expand, and contract more compared to the metallic PIP systems in the same level of temperature change. All PIP systems with a thickness of at least 3.178 mm (1/8 in) will not buckle at a temperature change of 22 °C (39.6 °F) except when the pipe length exceeds 170 in. (14 ft).
- The thickness required for PIP systems to resist the design internal pressure decreases with the increase of elastic modulus. A thickness of 3.175 mm (1/8 in.), the elastic modulus of 1 GPa and allowable hoop strain of 0.02 is sufficient to resist the internal pressure of 60 psi but should be increased to 6.35 mm (2/8 in.) and 12.7 mm (4/8 in.) to safely resist an internal pressure of 100 psi and 200 psi, respectively. A wall thickness of 3.175 mm (1/8 in.) will resist the design internal pressure of 200 psi, 100 psi and 60 psi if the PIP systems have an elastic modulus of at least 70 GPa (10,153 ksi), 24.5 GPa (3553 ksi) and 15 GPa (2176 ksi), respectively when the allowable hoop strain is at 0.002.
- The elastic modulus and thickness of PIP systems have a significant effect on the failure modes under impact loading. High modulus and thick PIPs will be dented under impact while the impact loads will penetrate high modulus and thin PIPs. A thickness of 9.525 mm (0.375 in) and higher is required for PIP system with an elastic modulus of 1 GPa (145 ksi) under impact loading while a thickness of at least 12.7 mm (0.5 in) is required for metallic PIP systems.
- The AHP suggested that the lateral deformation (PO2) is the most critical PO based on global priority as well as both criteria (thickness and elastic modulus of PIP system) for all the design pressure of 60, 100 and 200 psi. Impact load (PO6), vibration load (PO1), axial deformation (PO4), hoop stress (PO5), and cross-section ovalization (PO3), respectively, is the global ranking for the rest of critical POs when the design pressure is considered as 60 psi. On the other hand, the global ranking of the rest of the critical POs for the PIP system is PO6, PO5, PO4 and PO3, respectively, when the design pressure is considered as 100 psi and PO5, PO6, PO4 and PO3, respectively when the design pressure considered as 200 psi. Cross-section ovalization is found to be the least critical PO of the PIP system for any design internal pressure.

It is important to note that the above conclusions are derived based on the attributes considered for each simulated PO. Moreover, the design properties established from these analyses should be the projected 50-year properties of the PIP systems and without the influence of the host pipes. Nonetheless, the approaches and results implemented in this study provide a framework for preliminary design of new PIP material systems for pipeline repair and rehabilitation. Moreover, the FE models and analytical analysis developed in this study can be applied to other PIP systems with different diameters and material properties. A more detailed analysis can also be implemented using the complete stress–strain behaviour of PIP material systems obtained according to appropriate ASTM Standards. Once new PIP systems are developed, the reliability and accuracy of the developed models can be validated from the results of the experimental tests.

Declaration of Competing Interest

The authors declare that they have no known competing financial interests or personal relationships that could have appeared to influence the work reported in this paper.

Acknowledgements

The information, data, or work presented herein was funded in part by the Advanced Research Projects Agency-Energy (ARPA-E), U.S. Department of Energy, under Award Number DE-AR0001327. The views and opinions of authors expressed herein do not necessarily state or reflect those of the United States Government or any agency thereof.

References

- [1] U.S. Energy Information Administration, 2021. <https://www.eia.gov/dnav/ng/ng_cons_num_dcu_nus_a.htm> (Accessed October 12, 2021).
- [2] Rapid Encapsulation of Pipelines Avoiding Intensive Replacement n.d. <<https://arpa-e.energy.gov/technologies/programs/repair/>> (Accessed October 12, 2021).
- [3] Yeun J. Jung, Sunil K. Sinha, Evaluation of trenchless technology methods for municipal infrastructure system, *J. Infrastruct. Syst.* 13 (2) (2007) 144–156.
- [4] M.V. Biezma, M.A. Andrés, D. Agudo, E. Briz, Most fatal oil & gas pipeline accidents through history: a lessons learned approach, *Eng. Fail. Anal.* 110 (2020) 1–14, <https://doi.org/10.1016/j.engfailanal.2020.104446>.
- [5] Pipeline Accident Report: Pacific gas and electric company, Natural gas transmission pipeline rupture and fire San Bruno, California, National Transportation Safety Board. Transportation (Amst), 2010.

- [6] Hongfang Lu, Saleh Behbahani, Mohammadamin Azimi, John C. Matthews, Shuai Han, Tom Iseley, Trenchless construction technologies for oil and gas pipelines: state-of-the-art review, *J. Constr. Eng. Manag.* 146 (6) (2020) 03120001, [https://doi.org/10.1061/\(ASCE\)CO.1943-7862.0001819](https://doi.org/10.1061/(ASCE)CO.1943-7862.0001819).
- [7] Board S. Pipeline accident report. NTS Board, Washington, DC, USA, NTSB/PAR-12/01 PB2012-916501, 2010.
- [8] A. Amirat, A. Mohamed-Chateaneuf, K. Chaoui, Reliability assessment of underground pipelines under the combined effect of active corrosion and residual stress, *Int. J. Press. Vessel Pip.* 83 (2) (2006) 107–117.
- [9] M. Najafi, Pipeline rehabilitation systems for service life extension. *Serv. life Estim. Ext. Civ. Eng. Struct.*, Elsevier, 2011, p. 262–289.
- [10] M. Witek, Gas transmission pipeline failure probability estimation and defect repairs activities based on in-line inspection data, *Eng. Fail. Anal.* 70 (2016) 255–272, <https://doi.org/10.1016/j.engfailanal.2016.09.001>.
- [11] Emilia Kuliczowska, Andrzej Kuliczowski, Barbara Tchorzewska-Cieślak, The structural integrity of water pipelines by considering the different loads, *Eng. Fail. Anal.* 118 (2020) 104932, <https://doi.org/10.1016/j.engfailanal.2020.104932>.
- [12] Md Shamsuddoha, Allan Manalo, Thiru Aravinthan, Md Mainul Islam, Luke Djukic, Failure analysis and design of grouted fibre-composite repair system for corroded steel pipes, *Eng. Fail. Anal.* 119 (2021) 104979, <https://doi.org/10.1016/j.engfailanal.2020.104979>.
- [13] V.M. Karbhari, *Rehabilitation of Pipelines Using Fiber-Reinforced Polymer (FRP) Composites*, Elsevier, 2015.
- [14] Sirimanna CS, Manalo AC, Karunasena W, Banerjee S, McGarva L. Fiber-reinforced polymer (FRP) repair systems for corroded steel pipelines. *Rehabil. Pipelines Using Fiber-reinforced Polym. Compos.*, Elsevier, 2015, p. 267–285.
- [15] Xudong Gao, Yongbo Shao, Cheng Chen, Hongmei Zhu, Kangshuai Li, Experimental and numerical investigation on transverse impact resistance behaviour of pipe-in-pipe submarine pipelines after service time, *Ocean Eng.* 248 (2022) 110868, <https://doi.org/10.1016/j.oceaneng.2022.110868>.
- [16] F. Davaripour, B.W.T. Quinton, K. Pike, An assessment on the plastic capacity of pipe-in-pipe systems under damage progression effect, *J. Appl. Mech. Trans. ASME* 88 (2021) 1–12, <https://doi.org/10.1115/1.4049422>.
- [17] W.A. Oke, O.A. Adeyemi, A.O. Salau, Investigation of approximate mode shape and transition velocity of pipe conveying fluid in failure analysis, *Adv. Mech. Eng.* 14 (2022) 1–24, <https://doi.org/10.1177/16878140211072410>.
- [18] Z. Li, L. Wang, Z. Guo, H. Shu, Elastic buckling of cylindrical pipe linings with variable thickness encased in rigid host pipes, *Thin-Wall. Struct.* 51 (2012) 10–19, <https://doi.org/10.1016/j.tws.2011.11.003>.
- [19] Sang-Soo Jeon, Thomas D. O'Rourke, Anil N. Neravali, Repetitive loading effects on cast iron pipelines with cast-in-place pipe lining systems, *J. Transp. Eng.* 130 (6) (2004) 692–705, [https://doi.org/10.1061/\(ASCE\)0733-947X\(2004\)130:6\(692\)](https://doi.org/10.1061/(ASCE)0733-947X(2004)130:6(692)).
- [20] B. Guo, S. Song, A. Ghalambor, T.R. Lin, J. Chacko, *Offshore Pipelines*, Elsevier, 2005.
- [21] Ahmet Samanci, Ahmet Avci, Necmettin Tarakcioglu, Ömer Sinan Şahin, Fatigue crack growth of filament wound GRP pipes with a surface crack under cyclic internal pressure, *J. Mater. Sci.* 43 (16) (2008) 5569–5573, <https://doi.org/10.1007/s10853-008-2820-x>.
- [22] Yanmei Zhang, Zhongmin Xiao, Jun Luo, Fatigue crack growth investigation on offshore pipelines with three-dimensional interacting cracks, *Geosci. Front.* 9 (6) (2018) 1689–1697, <https://doi.org/10.1016/j.gsf.2017.09.011>.
- [23] P. Arora, S.K. Gupta, P.K. Singh, V. Bhasin, K.K. Vaze, A.K. Ghosh, et al., Fatigue crack initiation and crack growth studies for pipes made of carbon steel, *React. Technol.* (2009) 1–8.
- [24] V.E. Melissianos, D. Vamvatsikos, C.J. Gantes, Performance-based assessment of protection measures for buried pipes at strike-slip fault crossings, *Soil Dyn. Earthq. Eng.* 101 (2017) 1–11, <https://doi.org/10.1016/j.soildyn.2017.07.004>.
- [25] P. Vazouras, S.A. Karamanos, P. Dakoulas, Mechanical behavior of buried steel pipes crossing active strike-slip faults, *Soil Dyn. Earthq. Eng.* 41 (2012) 164–180, <https://doi.org/10.1016/j.soildyn.2012.05.012>.
- [26] Akbar Vasseghi, Ebrahim Haghshenas, Aram Soroushian, Masoumeh Rakhshandeh, Failure analysis of a natural gas pipeline subjected to landslide, *Eng. Fail. Anal.* 119 (2021) 105009, <https://doi.org/10.1016/j.engfailanal.2020.105009>.
- [27] W. Liu, Q. Guo, C. Qiao, W. Hou, Strain design method of buried pipeline crossing fault, *Eng. Fail. Anal.* 105 (2019) 659–671, <https://doi.org/10.1016/j.engfailanal.2019.07.036>.
- [28] S. Budhe, M.D. Banea, S. de Barros, Composite repair system for corroded metallic pipelines: an overview of recent developments and modelling, *J. Mar. Sci. Technol.* 25 (4) (2020) 1308–1323, <https://doi.org/10.1007/s00773-019-00696-3>.
- [29] H.S. da Costa Mattos, J.M.L. Reis, L.M. Paim, M.L.D. da Silva, R. Lopes Junior, V.A. Perrut, Failure analysis of corroded pipelines reinforced with composite repair systems, *Eng. Fail. Anal.* 59 (2016) 223–236, <https://doi.org/10.1016/j.engfailanal.2015.10.007>.
- [30] H.S. Da Costa Mattos, L.M. Paim, J.M.L. Reis, Analysis of burst tests and long-term hydrostatic tests in produced water pipelines, *Eng. Fail. Anal.* 22 (2012) 128–140, <https://doi.org/10.1016/j.engfailanal.2012.01.011>.
- [31] H.E. Stewart, S. Weinberg, B.A. Berger, J.E. Strait, Slow Cooling of Cured-in-Place Liners for Cast Iron and Steel Gas Pipelines 2019, 86.
- [32] H.E. Stewart, T.D. O'Rourke, B.P. Wham, A.N. Netravali, C. Argyrou, X. Zeng, et al., Performance testing of field-aged cured-in-place liners (CIPL) for cast iron piping. Final Rep Prep NYSEARCH/Northeast Gas Assoc December, Cornell Univ 2015.
- [33] D2412 A. Standard Test Method for Determination of External Loading Characteristics of Plastic Pipe by Parallel-Plate Loading. *Annu. B ASTM Stand.* 02 (2009) 2–7. <<https://doi.org/10.1520/D2412-21.2>>.
- [34] Geon Ho Lee, Hassan Pouraria, Jung Kwan Seo, Jeom Kee Paik, Burst strength behaviour of an aging subsea gas pipeline elbow in different external and internal corrosion-damaged positions, *Int. J. Nav. Archit. Ocean Eng.* 7 (3) (2015) 435–451, <https://doi.org/10.1515/ijnaoe-2015-0031>.
- [35] W.J. Stronge, S. Kobayashi, M. Kawahara, S. Wakayama, S. Kobayashi, T. Imai, et al., The effect of stress ratio on the fracture morphology of filament wound composite tubes, *Mater. Des.* 43 (2013) 471–484, <https://doi.org/10.1016/j.matdes.2013.01.026>.
- [36] The Engineering Toolbox, Temperature Expansion Coefficients common Piping Materials. n.d. <https://www.engineeringtoolbox.com/pipes-temperature-expansion-coefficients-d_48.html> (Accessed October 12, 2021).
- [37] ASME PCC-2-2018, Repair of Pressure Equipment and Piping, Article 401 – Nonmetallic Composite Repair System for Pipelines and Pipe works: High Risk Applications, American Society of Mechanical Engineers, 2018.
- [38] Simulia DS. ABAQUS/CAE 6.21. ABAQUS Anal Theory Manuals, SIMULIA, Dassault Systèmes, Realis Simulation, Provid RI, USA, 2021.
- [39] Ansys, Finite Element Analysis (FEA) Software for Structural Engineering, 2021.
- [40] Pipeline and Hazardous Materials Safety Administration (PHMSA). Incident Reports Database, n.d.
- [41] Y. Gorash, D. Mackenzie, On cyclic yield strength in definition of limits for characterisation of fatigue and creep behaviour, *Open Eng.* 7 (2017) 126–140, <https://doi.org/10.1515/eng-2017-0019>.
- [42] H.E. Stewart, T.D. O'Rourke, B.P. Wham, A.N. Netravali, C. Argyrou, X. Zeng et al., Technology Transfer Demonstrations and Post-Mortem Testing of Cast Iron and Steel Pipe Lined with Cured-in-Place Liners (CIPL), 2015.
- [43] T. Tafsirojijaman, S. Fawzia, D.P. Thambiratnam, X.L. Zhao, Study on the cyclic bending behaviour of CFRP strengthened full-scale CHS members, *Structures* 28 (2020) 741–756, <https://doi.org/10.1016/j.istruc.2020.09.015>.
- [44] T. Tafsirojijaman, S. Fawzia, D. Thambiratnam, X. Zhao, Numerical investigation of CFRP strengthened RHS members under cyclic loading, *Structures* 24 (2020) 610–626, <https://doi.org/10.1016/j.istruc.2020.01.041>.
- [45] T. Tafsirojijaman, S. Fawzia, D.P. Thambiratnam, Investigation on the behaviour of CFRP strengthened CHS members under Monotonic loading through finite element modelling, *Structures* 28 (2020) 297–308, <https://doi.org/10.1016/j.istruc.2020.08.059>.
- [46] *Inspection Practices for Piping System Components Inspection Practices for Piping System Components*. Api Recomm. Pract., 1998.
- [47] Saaty TL, Alexander JM. L. g. vargas. 2001. Models, methods, concepts & applications of the analytic hierarchy process, n.d.
- [48] Peng Yu, Allan Manalo, Wahid Ferdous, Rajab Abousnina, Choman Salih, Tom Heyer, Peter Schubel, Investigation on the physical, mechanical and microstructural properties of epoxy polymer matrix with crumb rubber and short fibres for composite railway sleepers, *Constr. Build. Mater.* 295 (2021) 123700, <https://doi.org/10.1016/j.conbuildmat.2021.123700>.
- [49] W. Ferdous, A. Manalo, T. Aravinthan, G. Van Erp, Properties of epoxy polymer concrete matrix: effect of resin-to-filler ratio and determination of optimal mix for composite railway sleepers, *Constr. Build. Mater.* 124 (2016) 287–300, <https://doi.org/10.1016/j.conbuildmat.2016.07.111>.

- [50] M. Velasquez, P. Hester, An analysis of multi-criteria decision making methods, *Int. J. Oper. Res.* 10 (2013) 56–66.
- [51] S. Nataraj, Analytic Hierarchy Process As a Decision-Support system in the petroleum pipeline industry, *Inf. Syst.* VI (2005) 16–21.
- [52] J. Wan, G. Qi, Z. Zeng, S. Sun, The application of AHP in oil and gas pipeline route selection, in: *Proc – 2011 19th Int. Conf. Geoinformatics, Geoinformatics 2011 2011*, pp. 1–4. <<https://doi.org/10.1109/GeoInformatics.2011.5981038>>.
- [53] Z. Wu, G. Abdul-Nour, Comparison of multi-criteria group decision-making methods for urban sewer network plan selection, *CivilEng 1* (2020) 26–48, <https://doi.org/10.3390/civileng1010003>.
- [54] A.N. Netravali, T.D. O'Rourke, K.I. Gerretisen, Y.P. Singh, S.S. Jeon, D. Zhao, *Advanced Pipeline Support and Stabilized Backfill for Gas Mains. Final Rep Contract No 31120, Prep New York Gas Group, Cornell Univ, 2000.*
- [55] T.D. O'Rourke, D.T. Grubb, A.N. Netravali, CHT, Evaluating service life of cast iron joint sealing products and techniques. *Geotech. Eng. Rep. 85 3, Sch. Civ. Environ. Eng. Cornell. Univ. Ithaca, NY, May 1985.*
- [56] T.D. O'Rourke, A.N. Netravali, S.M. Pendharkar, A. Tonkinson, D. Chaudhuri and ST. Evaluating Service Life of Anaerobic Joint Sealing Products and Techniques. *Final Rep GRI-96/0318, Gas Res Institute, Chicago, IL, Sept 1996.*